Final Draft

of the original manuscript

Kreuzer, L.; Widmann, T.; Aldosari, N.; Bießmann, L.; Mangiapia, G.; Hildebrand, V.; Laschewsky, A.; Papadakis, C.; Müller-Buschbaum, P.:

Cyclic Water Storage Behavior of Doubly Thermoresponsive Poly(sulfobetaine)-Based Diblock Copolymer Thin Films.

In: Macromolecules. Vol. 53 (2020) 20, 9108 - 9121.
First published online by ACS: 14.10.2020

https://dx.doi.org/10.1021/acs.macromol.0c01335

Cyclic Water Storage Ability in Doubly Thermo-responsive Poly(sulfobetaine)-Based Diblock Copolymer Thin Films

Lucas P. Kreuzer[†], Tobias Widmann[†], Nawarah Aldosari[†], Lorenz Bießmann[†], Gaetano Mangiapia[§], Viet Hildebrand[‡], André Laschewsky[‡,⊥], Christine M. Papadakis[†], Peter Müller-Buschbaum[†,$,]*

[†]Lehrstuhl für Funktionelle Materialien, Physik Department, Technische Universität München, James-Franck-Str. 1, 85748 Garching, Germany

[§]Helmholtz-Zentrum Geesthacht at Heinz Maier-Leibnitz Zentrum, Lichtenbergstr. 1, 85747 Garching, Germany

[‡]Institut für Chemie, Universität Potsdam, Karl-Liebknecht-Str. 24-25, 14476 Potsdam-Golm, Germany

[⊥]Fraunhofer Institut für Angewandte Polymerforschung, Geiselbergstr. 69, 14476 Potsdam-Golm, Germany

[$]Heinz Maier-Leibnitz Zentrum (MLZ), Technische Universität München, Lichtenbergstr. 1, 85748 Garching, Germany

KEYWORDS: poly(sulfobetaine), doubly thermo-responsive thin film, cyclic swelling, neutron scattering

* E-mail Corresponding author: muellerb@ph.tum.de

Abstract

The cyclic swelling and collapse behavior of a doubly thermoresponsive diblock copolymer thin film, consisting of a zwitterionic poly(sulfobetaine), poly(*N*,*N*-dimethyl-*N*-(3-methacrylamidopropyl)-ammoniopropane sulfonate) (PSPP), and a nonionic poly(*N*-isopropylmethacrylamide) (PNIPMAM) block, is investigated *in situ* at three characteristic temperatures with time-of-flight neutron reflectometry. With increasing temperature, the thin film becomes less hydrophilic, which leads to a decreased but faster water uptake. This response of the block copolymers in the thin-film geometry differs greatly from their known aqueous solution behavior. In the cyclic experiments at constant temperature, the behavior is reproducible in terms of mesoscopic parameters such as swelling ratio and water content, even though Fourier transform infrared spectroscopy reveals altered swelling mechanisms, which are attributed to a complex interplay between different water species. Thus, the overall reduced hydrophilicity affects the overall swelling behavior of the thin film but not the hydration of particular functional groups of the diblock copolymer PSPP-b-PNIPMAM.

1. Introduction

Polymer thin films are widely used in the fields of artificial pumps and muscles, [1,2] nanosensors, and switches [3−10] or as coatings in order to generate functionalized surfaces.[11−15] Inevitably, the thin films are exposed to a surrounding atmosphere, which in most cases is air, containing a certain fraction of H_2O molecules, which can easily penetrate into the polymer thin film, resulting in altered film properties. Usually, the diffusion of water into the film, which is driven by the osmotic pressure, is accompanied by swelling and plasticization of the polymer. Therefore, the polymer thin film becomes thicker and softer.[16−18] With respect to applications, the increase in volume can be exploited, for example, to close gaps, move objects or for sensing purposes.[19−21] Importantly, thin films have very short response times.[22−24] In addition, the interfacial areas play an important role, and both the substrate−polymer and polymer−air interfaces affect the diffusion process. Thus, it is more complex and cannot be extrapolated from the well-studied diffusion processes of the respective bulk materials.[25−29]

An elegant way to induce the absorption and release of small molecules is the use of stimuli-responsive materials, which react strongly to external stimuli such as temperature, relative humidity (RH), illumination, and salt concentration.[30−37] Hence, parameters that are easy to control, for example, temperature or RH, can be used to change the mechanical properties and the dimensions of a thin film from responsive polymers. Representatives of the class of thermoresponsive polymers are poly(sulfobetaine)s (PSBs), which in aqueous solution, show a miscibility gap below their upper critical solution temperature (UCST).[38−42] This is highly unusual as UCST-like behavior is rather observed for polymers in organic solvents but not in aqueous solvents.[43,44] Other zwitterionic polymers, such as poly(phosphatidylcholine)s and poly-(carboxybetaine)s, are generally not thermoresponsive in aqueous solution.[45−48] In addition to their special solution behavior, their high biocompatibility qualifies PSBs as antifouling coatings and for biomedical applications.[15,49−52] In contrast, nonionic thermoresponsive polymers, such as poly(*N*-isopropylacrylamide) and poly(*N*-isopropylmethacrylamide) (PNIPMAM), usually show

a miscibility gap above their lower critical solution temperature (LCST), which is the result of changes in hydrophilicity and the number of hydrogen bonds between water molecules and the polymer chains.[53−55]

By combining appropriate LCST- and UCST-type homopolymers with each other, diblock copolymers (DBCs) are created, which show unique solution behavior. The chemical structure of such a PSB-based DBC (PSPP-b-PNIPMAM) is shown in Figure 1a.

In aqueous solution, they can self-assemble into micelles with a hydrophobic core and a hydrophilic shell in different ways. Upon temperature change, the micelle structure can be reversed, implying that the hydrophobic core becomes the hydrophilic shell and vice versa. This behavior is often called "schizophrenic" micellar self-assembly and is shown in Figure 1b.[56−61] An intermediate regime is present, which is either fully hydrophilic or fully hydrophobic, dependent on the relative positions of the cloud point of the PNIPMAM block (CP_{LCST}) and the clearing point of the PSB block (CP_{UCST}). In aqueous solution, the CP_{UCST} of PSB is strongly affected by the polymer concentration, the H−D isotope effect (CP_{UCST} increases in D_2O), and salt additives (CP_{UCST} first increases and then decreases). Therefore, it is possible to realize an inversion of the micellar core−shell structure via the fully miscible regime, via the fully immiscible regime, or directly.[57−60,62,63] In the thin-film geometry, the polymer concentration can be controlled by the absorption and release of water molecules. During water absorption, the polymer concentration decreases. In contrast, the polymer concentration is increased during the collapse process because water molecules are expelled from the thin film. The interactions induced by the interfaces due to the thin-film geometry possibly cause a shift of both the respective UCST and LCST, as was reported recently.[64] Therefore, these doubly thermoresponsive PSB-based DBCs react differently in the thin-film geometry and in aqueous solutions with respect to changes in temperature. Moreover, the response of the thin films to these changes differs, whether they are in a fully or only partly swollen state.

Besides the fundamental understanding of the absorption and release mechanisms of the respective gaseous or liquid molecules into and out of thin films, which is still a rare topic in the literature,[35,40,64,65] a reproducible swelling and collapse process is of equally high importance. In particular, swelling with water molecules is interesting for thermoresponsive polymers.

In our work, we investigate in how far the absorption and release mechanisms with respect to the change in film thickness and water uptake are reproducible in three full consecutive cycles of swelling and drying. Because of the multiple thermoresponsiveness of the DBC thin film, the swelling and collapse behavior can be altered by choosing different temperatures. Therefore, the system gains even more flexibility and enables a wider use in applications than simple thermoresponsive systems. Cyclic swelling and drying of thermoresponsive polymer thin films at constant temperature were already addressed by some of us before[18]; however, we are not aware of any studies addressing thin films from DBCs that feature both an LCST-type block and an UCST-type block. Furthermore, the effect of temperature on the cyclic water swelling and drying behavior has, to the best of our knowledge, not been reported in the literature before. In the present study, we investigate the cyclic water swelling behavior of a DBC thin film at three temperatures, that is, at [15, 27], and 48 °C, which are characteristic for different solution scenarios of the constituting blocks. The DBC consists of a zwitterionic poly(*N*,*N*-dimethyl-*N*-(3-methacrylamidopropyl)-ammoniopropane sulfonate) (PSPP) block and a nonionic PNIPMAM block (Figure 1a). According to our previous work on aqueous solutions of such a DBC, the three chosen temperature values represent the following regimes:58 (i) 15 °C is below both CP_{UCST} and CP_{LCST}, (ii) 27 °C is above the CP_{UCST} but below the CP_{LCST}, and (iii) 48 °C is above both CP_{UCST} and CP_{LCST} of the DBC in aqueous solution. Thus, these values are selected as starting temperatures for the three individual experiments. It was seen recently that these regimes might shift when changing the sample system to a thin-film geometry.[64] We use time-of-flight neutron reflectometry (ToF-NR) to follow the kinetics during three swelling and drying cycles at each of the chosen temperatures in situ. With this scattering technique, mesoscopic parameters such as

film thickness, scattering length density (SLD), and film roughness are monitored as a function of time. In order to maximize the contrast in SLD between the DBC and the water molecules, D_2O is used during all swelling cycles. From the SLD, not only the overall water content Φ is calculated but also the entire vertical film composition profile, which gives detailed information about the location of D_2O molecules in the thin film during the swelling and drying processes, is determined. The amount of absorbed and released water as well as the final change in film thickness can be compared among the three swelling and drying cycles, and the impact of an altered ambient temperature on the swelling and drying process is investigated.

In addition, Fourier transform infrared (FTIR) spectroscopy is applied in situ to probe changes in polymer−water interactions upon swelling. Deuteration processes are monitored because especially the hydrogen atom in the amide group, which is present in both blocks, the PSPP and

PNIPMAM block, is sufficiently acidic to be easily exchanged by a deuterium atom from the penetrating D_2O molecules. Also, the behavior of characteristic groups such as the SO_3^- group at the end of the PSPP side chains is analyzed with FTIR spectroscopy. Hence, detailed information about the swelling mechanism over three swelling cycles at different temperatures is not only obtained on the whole polymer thin film but also obtained on the particular groups.

2. Introduction

2.1. Materials. The synthesis of poly(*N*,*N*-dimethyl-*N*-(3- methacrylamidopropyl)-ammoniopropane sulfonate)-block-poly(*N*-isopropylmethacrylamide) ($PSPP_{500}$-b-$PNIPMAM_{150}$) was described before.[58] Deuterated water (D_2O, Armar, 99.9 atom % D, used for synthesis and characterization, Deutero GmbH, purity 99.95%), dichloromethane-d_2 (CD_2Cl_2, Armar, 99.5 atom % D), diethyl ether (VWR, 100%), methanol (Avantor, 99%), sodium chloride (ChemSolute, 99%), and 2,2,2-trifluoroethanol (TFE, Roth, 99.8%) were used without further treatment. Water was used for cleaning purposes after purification (Millipore Milli-Q Plus, a resistivity of 18.2 MΩ cm^{-1}).

2.1.1. Sample Preparation for ToF-NR and Spectral Reflectance. Silicon with a thin oxide layer on the surface was used as a substrate for PSPP-b-PNIPMAM thin films. The substrate was precut and subsequently cleaned in an acidic bath (54 mL of H_2O, 84 mL of H_2O_2, and 198 mL of H_2SO_4 for 15 min at 80 °C). The substrates were rinsed with Millipore water to remove possible traces of the acidic bath. By treating the substrate surface with oxygen plasma (200 W for 10 min), it turned hydrophilic. Water-free PSPP-b-PNIPMAM thin films were prepared by spin coating (2500 rpm for 900 s) out of the TFE solution at 25 °C. Solvent vapor annealing (900 s) in a saturated TFE atmosphere resulted in very smooth and homogeneous thin film surfaces.

2.1.2. Sample Preparation for FTIR Spectroscopy. Precut silicon substrates were treated with oxygen plasma (200 W for 10 min). After a waiting time of 25 min, the water-free PSPP-b-PNIPMAM thin films were drop-cast from the TFE solution onto the substrates, followed by drying and storage in a desiccator. The drop-casting technique results in thicker films and a domelike droplet shape, which improves the quality of the FTIR signal.

2.2. Methods. 2.2.1. Time-of-Flight Neutron Reflectometry. NR experiments were carried out using the REFSANS instrument at the Heinz Maier-Leibnitz Zentrum (MLZ) in Garching, Germany.[66,67] The incoming neutrons had wavelengths from 3 to 21 Å and a resolution of $\Delta\lambda/\lambda$ = 1.6% for static measurements and $\Delta\lambda/\lambda$ = 3.1% for kinetic measurements. The ToF mode was applied. For static measurements, two fixed incident angles, $\alpha_i = 0.6$ deg (a 20 min measuring time) and $\alpha_i = 2.4$ deg (100 min), were used in order to cover a large *q*-range. Kinetic measurements were performed at a fixed angle of $\alpha_i = 0.76$ deg with a time binning of 30 s. The sample−detector distance was 10.32 m. For all measurements, the sample was mounted in a custom-made humidity chamber, which was connected to a JULABO FP 50 thermal bath (JULABO Labortechnik GmbH, Seelbach, Germany) to ensure temperature control. RH was controlled by connecting the sample chamber to a custom-made gas flow system. Dry nitrogen is led either directly to the chamber (for drying) or through two washing bottles filled with D2O

before reaching the chamber (for swelling). This allowed for a fast and precise adjustment of the RH. The evolution of temperature and RH was followed with a SHT31 humidity and temperature sensor (Sensirion AG, Staefa, Switzerland). Both static and kinetic ToF-NR data were analyzed using a three-layer model within the framework of the Motofit package, yielding the film thickness and the average SLD of the DBC thin film.[68]

2.2.2. FTIR Spectroscopy. FTIR measurements were conducted using an Equinox FTIR spectrometer (Bruker, Billerica, United States) equipped with a DTGS detector. The data were averaged over 256 scans in total over a range of wavenumbers of 600−4000 cm^{-1} with a resolution of 2 cm^{-1}. The measurement cell was constantly purged by dried and CO_2-filtered air in order to exclude H_2O and CO_2 molecules from the pathway of the IR beam. To enable in situ measurements, a custom-made sample environment was used, as was already described in our previous work.[35,64,65] Thermal control was assured using a JULABO F12 MC thermal bath. The RH and temperature within the sample environment were tracked with a SHT31 humidity and temperature sensor. For kinetic studies, FTIR measurements were performed every 30 min.

2.2.3. Spectral Reflectance. The thin-film thickness was measured using a Filmetrics F20 ThinFilm Measurement System (Filmetrics Inc., San Diego, United States). The thin film on a Si substrate was placed horizontally on a sample stage in a custom-made sample environment for RH and temperature control, as was already described in our previous work.[35,64,65] The sample stage was surrounded by a reservoir. Injection of D_2O in this reservoir increased the RH in the sample chamber. Thermal control was assured by connecting the chamber to a JULABO F12 MC thermal bath. Both parameters, RH and temperature, were tracked with a SHT31 humidity and temperature sensor. The incoming light passed through a CaF_2 window in the lid of the chamber and illuminated the sample from the top. The resulting interference pattern was analyzed by model fitting. The best fits were achieved by using a three-layer model.

3. Results and Discussion

The experimental protocol is depicted in Scheme 1. Three swelling and drying cycles at 15 °C (Scheme 1a), 27 °C (Scheme 1b), and 48 °C (Scheme 1c) are followed in situ with ToF-NR. At the beginning, the as-prepared $PSPP_{500}$-b-$PNIPMAM_{150}$ thin film is probed with static ToF-NR. Next, the RH of D_2O inside the chamber is increased (>90%), which induces the swelling process. The swelling kinetics is followed with in situ ToF-NR with a time resolution of 30 s. A second static NR measurement is done on the swollen DBC thin film. After that, the RH is decreased (to 0%), while the drying kinetics is monitored with in situ ToF-NR. A final static measurement of the dried DBC thin film terminates one swelling and drying cycle. In total, three such cycles are conducted at each temperature (15, 27, and 48 °C). In addition to the ToF-NR measurements, FTIR spectroscopy and spectral reflectance (SR) are used to monitor three swelling cycles in situ at the aforementioned temperatures. The RH and the temperature profiles as a function of time over all three swelling and drying cycles are shown in Figure S1 in the Supporting Information. After inducing the kinetic processes, the RH changes rapidly (ca. 10 min), from 0% to above 85% for the swelling process and from above 90% to below 5% for the drying process.

3.1. Swelling Behavior. The swelling behavior of the DBC thin films is investigated with SR. The experimental design is analogous to ToF-NR experiments (cf. Scheme 1), and the results are shown in Figure S2. A lower swelling ratio d/d_{ini} at higher temperatures is observed, indicating a general trend of lower hydrophilicity at higher temperatures. This behavior is highly unexpected because the water vapor pressure is strongly increased at higher temperatures, and from the phase behavior of the aqueous solution, we expect the lowest hydrophilicity at 15 °C (the PNIPMAM block is hydrophilic, but the PSPP block, which has the significantly higher molar mass, is water-insoluble), the highest hydrophilicity at 27 °C (both blocks are water-soluble), and an intermediate hydrophilicity at 48 °C (the PSPP block is water-soluble, but the PNIPMAM block is insoluble). To further analyze the temporal evolution of the swelling ratio d/d_{ini}, a swelling model is applied to the data. The model respects the intrinsic, diffusion-driven swelling kinetics as well as a

nonconstant RH (Figure S1), whereas polymer−substrate interactions are not included. From this model, the effective Flory−Huggins interaction parameter χ_{eff} and the time constant τ are extracted. χ_{eff} describes the interaction between water and the DBC without the interaction ns of the DBC with the substrate and therefore cannot be seen as an absolute Flory−Huggins parameter under certain environmental conditions. The time constant τ yields information about the timescales of the occurring diffusion processes. Both extracted parameters are obtained by investigating either a swelling process or a drying process. Hence, these values describe the corresponding dynamic process, regarding the change in film thickness (via SR and ToF-NR) and water content (ToF-NR and FTIR), in relation to the RH. A detailed explanation of the model, together with the underlying eqs S1−S4 can be found in our previous work and in the Supporting Information.[35,64,65] All values for χ_{eff} and τ given in the following are extracted from the first swelling cycle at the corresponding temperature unless stated otherwise. When the swelling model is applied to the SR data, the observed trend of a lower hydrophilicity at higher temperatures is confirmed (all extracted parameters are summarized in Table S1 in the Supporting Information). The obtained $\chi_{eff}\left(d/d_{ini}\right)$ parameter is (0.60 ± 0.02) at 15 °C, (0.91 ± 0.02) at 27 °C, and (1.12 ± 0.04) at 48 °C. The resulting $\tau\left(d/d_{ini}\right)$ values indicate a faster water uptake at higher temperatures: (30 ± 1) min at 15 °C, (20 ± 1) min at 27 °C, and (16 ± 1) min at 48 °C. This can be explained by reduced diffusion pathways because of a decreased swelling ratio d/d_{ini}. When comparing the end states of the individual swelling cycles, we observe that in the case of each first swelling cycle, a lower swelling ratio d/d_{ini} is reached as compared to the second and third swelling cycles. Changes in the polymer chain conformation become possible in the swollen films. Therefore, we attribute these changes in the water storage capacity of the films to an improved chain conformation of the DBC, regarding the amount of absorbed and released water. To

investigate the swelling behavior in more detail, ToF-NR is applied in situ according to Scheme 1.

Static ToF-NR measurements of the $PSPP_{500}$-b-$PNIPMAM_{150}$ DBC thin films in their as-prepared and redried states after each swelling cycle are shown in Figure 2. By fitting the reflectivity curves with a three-layer model, the total film thickness and average SLD are extracted. The corresponding values are listed in Table 1.

The three individual thin films in their as-prepared states have equal initial thicknesses within the precision of the measurements: (63 ± 3) nm at 15 °C, (65 ± 3) nm at 27 °C, and (60 ± 2) nm at 48 °C. In order to rule out slight variations, the film thickness d is normalized to its initial film thickness dini, thereby yielding the swelling ratio d/d_{ini}. Also, the average SLD values are rather similar: (0.91 ± 0.02) · 10^{-6} $Å^{-2}$ at 15 °C, (0.85 ± 0.01) · 10^{-6} $Å^{-2}$ at 27 °C, and (0.90 ± 0.02) · 10^{-6} $Å^{-2}$ at 48 °C. However, they are smaller than the theoretical SLD of the DBC (1.044 · 10^{-6} $Å^{-2}$).[69] This can be attributed to an altered chain conformation because of the film preparation via spin coating out of TFE as well as to the presence of water molecules. The average SLD is calculated from the SLD profile, which is determined from the fit to the NR data. As seen in Figure 2, the as-prepared DBC thin films show a homogeneous SLD distribution. Only in the case of the film used at 27 °C, a slightly nonhomogeneous SLD profile is found. After the swelling processes, the redried films have a very similar thickness as compared to the initial film thickness. However, all thin DBC films exhibit a heterogeneous SLD profile with lower SLD values close to the substrate−polymer and polymer−air interfaces and higher SLD values in the center of the thin DBC film. The increase in SLD in the center of the DBC may be due to residual D_2O molecules from

the earlier swelling process. In addition, the polymer chains undergo a selective partial deuteration (namely, the −CONH− moieties) during the swelling process with D_2O molecules. The increased deuterium content in the thin films after drying also contributes to an increased SLD.

The three swelling cycles at 15, 27, and 48 °C are monitored with in situ ToF-NR. Analogous to the static measurements, the reflectivity curves of these kinetic measurements are analyzed with a three-layer model, yielding the film thickness and SLD values during swelling and drying. Selected NR curves including the fits of each first swelling cycle at 15, 27, and 48 °C are shown in Figure S3 in the Supporting Information. The extracted film thickness d is normalized to its initial film thickness d_{ini}, to give the swelling ratio d/d_{ini}. The water content Φ within the thin film is calculated from the determined $\mathrm{SLD}_{meas}(t)$ at a measurement time t, the theoretical $\mathrm{SLD_{DBC}}$ of the DBC, and the $\mathrm{SLD_{D_2O}}$ of D_2O via

$$\Phi(t) = \frac{\mathrm{SLD}_{meas} - \mathrm{SLD_{DBC}}}{\mathrm{SLD_{D_2O}} - \mathrm{SLD_{DBC}}} \quad (1)$$

Both the swelling ratio d/d_{ini} and the water content Φ as a function of time are shown in Figure 3 for all three swelling cycles at 15 °C (Figure 3a,d), 27 °C (Figure 3b,e), and 48 °C (Figure 3c,f).

One general trend emerges: at higher temperatures, the water content Φ and the swelling ratio d/d_{ini} decrease because of a decreased hydrophilicity and favored polymer−polymer interactions. This confirms the results found with SR. Apparently, the thin-film geometry induced interactions with the substrate and air interfaces, which are responsible for a shift of the $\mathrm{CP_{UCST}}$ (of the PSPP block) and $\mathrm{CP_{LCST}}$ (of the PNIPMAM block). The results indicate that the $\mathrm{CP_{PSPP}}$ has not been crossed and the behavior of the PSPP block regarding the water uptake is unaltered throughout the entire temperature range, while the PNIPMAM block is already in a partly collapsed state at 27 °C and further collapsed at 48 °C. Hence, the PNIPMAM block exhibits a coil-to-globule collapse over a broad temperature range, which is in agreement with the behavior known from aqueous solutions. Because the chain mobility is lower in the thin-film geometry than in the solution, the transition range is even expected to become broader. Even though the water uptake decreases at higher temperatures, it occurs more rapidly because diffusion pathways are reduced and polymer−water interactions are not favored. Furthermore, it can be seen that D_2O molecules from

the first swelling cycle remain inside the DBC film as the respective second and third swelling cycles already start with an offset in the D_2O content. This effect is also partly caused by deuteration of the polymer chains. A change in chain conformation of the DBC thin film during the first swelling cycle of each run, as seen in the SR measurements, is also present in the ToF-NR experiments as the swelling ratio d/d_{ini} and the water content Φ reach higher values for the respective second and third swelling cycles. This is in contrary to previous results of cyclic swelling of thin films, where an aging process and eventually a decreased water storage capability were found.[18]

To further analyze the temporal evolution of the swelling ratio d/d_{ini} and the water content Φ, the swelling model is applied to the evolution of the swelling ratio and to the water content.[35,64,65] The values of χ_{eff} and τ that are extracted from the evolution of the swelling ratio d/d_{ini} confirm the trends that are already explained above (all χ_{eff} and τ values are listed in Table S2 in the Supporting Information). $\chi_{eff}\left(d/d_{ini}\right)$ increases at higher temperatures (0.32 ± 0.02 at 15 °C, 0.52 ± 0.01 at 27 °C, and 0.65 ± 0.03 at 48 °C), underlining that the DBC thin film becomes less hydrophilic, while $\tau\left(d/d_{ini}\right)$ decreases at higher temperatures (9 ± 1 min at 15 °C, 7 ± 1 min at 27 °C, and 6 ± 1 min at 48 °C), indicating faster completed diffusion processes. The values of χ_{eff} and τ that are extracted from the evolution of the water content Φ follow the same trend [$\chi_{eff}\left(\Phi\right)$ amounts to (0.14 ± 0.01) at 15 °C, (0.42 ± 0.02) at 27 °C, and (0.55 ± 0.02) at 48 °C, while $\tau\left(\Phi\right)$ is (10 ± 1) min at 15 °C, (7 ± 1) min at 27 °C, and (4 ± 1) min at 48 °C]. The increasing χ_{eff} values upon increasing temperature underline the assumption stated earlier. Apparently, the CP_{PSPP} and $CP_{PNIPMAM}$ shift significantly in the thin-film geometry as compared to the aqueous solution. Furthermore, $\chi_{eff}\left(d/d_{ini}\right)$ and $\tau\left(d/d_{ini}\right)$ have lower values as compared to $\chi_{eff}\left(\Phi\right)$ and

$\tau(\Phi)$. This indicates that the film thickness increases more slowly than water molecule diffusion into the film, which is attributed to voids. These voids are filled first, while the film increases only slowly in film thickness. Once the voids are filled, water uptake results in an increase in film thickness. This behavior of thermoresponsive thin films is already known from the literature.[35,65,70−72] The increasing difference between $\chi_{eff}(d/d_{ini})$, $\tau(d/d_{ini})$ and $\chi_{eff}(\Phi)$, $\tau(\Phi)$ values that are extracted from the second and third swelling cycles results from the changes in chain conformation as discussed above. Hence, it takes longer times to fill up the voids before the film thickness starts to increase during the swelling cycle.

In addition to the evolution of the swelling ratio d/d_{ini} and the model fit, the maximum swelling ratio $d_{\max}/d_{ini}$ (eq S2 in the Supporting Information) is shown in Figure 3a−c, which describes the limit of the swelling ratio d/d_{ini} at a given RH and χ_{eff}. In the beginning, a significant offset between the swelling ratio d/d_{ini} and the maximum swelling ratio $d_{\max}/d_{ini}$ is visible, identifying the diffusion as limiting factor of the ongoing swelling process. At later stages, after approximately 10 min, both curves merge, indicating that now the swelling process is limited by the RH, that is, by the available water molecules. This is in good agreement with the evolution of the RH (cf. Figure S1 in the Supporting Information) as after 10 min, the RH has already reached above 90% and increases slowly until it reaches equilibrium.

At the end of the film swelling, static ToF-NR measurements of the swollen DBC thin films are performed. By fitting a threelayer model, the related SLD profiles are determined (Figure 4). The extracted total film thickness and average SLD are listed in Table 1.

Again, it is obvious that the DBC becomes overall less hydrophilic upon increasing temperature, as both the film thickness and SLD decrease. The film thickness amounts to (190 ± 4) nm at 15 °C, (110 ± 2) nm at 27 °C, and (87 ± 2) nm at 48 °C, while the SLD is (3.4 ± 0.05) · 10^{-6} Å^{-2} at 15 °C, (2.93 ± 0.04) · 10^{-6} Å^{-2} at 27 °C, and (2.65 ± 0.02) · 10^{-6} Å^{-2} at 48 °C. Furthermore, the

respective first swelling cycles show lower film thickness values than the second and third swelling cycles, which have already been seen in the kinetic ToF-NR data (Figure 3) and in the SR data (Figure S2). The SLD profiles reveal two D_2O enrichment layers, which are present at all swollen states at all three temperatures. One is located close to the Si substrate−polymer interface and one at the polymer−air interface. The presence of an enrichment layer near the substrate is well known from the literature and results from interactions between D_2O and the hydrophilic Si and SiO_2 layer.[35,65] As reported earlier, in the D_2O solution, the DBC forms hydrophobic PSPP spheres surrounded by a hydrophilic PNIPMAM shell at 15 and 27 °C. In contrast, at 48 °C, the structure was inverted and the PSPP block formed a hydrophilic shell around a hydrophobic PNIPMAM core.[58] However, in the thin-film geometry, PNIPMAM cylinders were embedded in a PSPP matrix.64 Thus, a hydrophilic and hydrated PSPP layer at the film surface may possibly explain he enrichment layer at the polymer−air interface. The thickness of the hydrophilic PSPP shell around the PNIPMAM core in the D_2O solution at 48 °C (15 ± 2 nm) was in a similar range as the enrichment layers observed here in the thin-film geometry at all temperatures. Furthermore, with increasing temperature, the enrichment layer remains relatively constant in thickness. Thus, the PSPP matrix within the thin film is presumably substantially hydrated over the entire temperature range. In contrast, the PNIPMAM block collapses, and thus, the overall thickness of the whole thin film decreases at higher temperatures.

3.2. Drying Behavior. The shrinkage of the DBC thin film is induced by decreasing the RH (Figure S1). Analogous to the swelling cycles, the three drying cycles at each temperature are followed via in situ ToF-NR with a time resolution of 30 s. Selected NR curves of each first drying cycle are shown together with the three-layer model fits in Figure S3. Figure 5 shows the extracted swelling ratio d/d_{ini} (Figure 5a−c) and water content Φ (Figure 5d−f) as a function of time.

The initial starting values at $t = 0$ of d/d_{ini} and Φ differ for the three different cycle temperatures because of the different final swollen states. Furthermore, each first drying cycle

starts at lower d/d_{ini} and Φ values because of a still denser DBC thin film. The analysis of the swelling kinetics reveals a decreasing hydrophilicity with increasing temperature. Therefore, we expect accelerated collapse kinetics with increasing temperature as polymer−water interactions become less favored. Indeed, the results show the slowest decrease of the swelling ratio d/d_{ini} and water content Φ at 15 °C. However, the fastest decrease in swelling ratio d/d_{ini} and water content Φ occurs at 27 °C, while an intermediate decrease is seen at 48 °C. The applied swelling model confirms the observed trend. The extracted τ values (Table S3 in the Supporting Information) indicate the fastest decrease in film thickness and the fastest water release at 27 °C, and the slowest at 15 °C. For the drying kinetics, the $\tau(d/d_{ini})$ values amount to (21 ± 2) min at 15 °C, (6 ± 1) min at 27 °C, and (15 ± 1) min at 48 °C, while the $\tau(\Phi)$ values are (35 ± 4) min at 15 °C, (10 ± 1) min at 27 °C, and (24 ± 1) min at 48 °C. Thus, intermediate values are found at the highest temperature of 48 °C, while the values are smaller at 27 °C and higher at 15°. However, $\chi_{eff}(d/d_{ini})$ and $\chi_{eff}(\Phi)$ values indicate a decreasing hydrophilicity with increasing temperature: $\chi_{eff}(d/d_{ini})$ is 0.91 ± 0.03 at 15 °C, 1.11 ± 0.04 at 27 °C, and 1.21 ± 0.05 at 48 °C, and $\chi_{eff}(\Phi)$ is 1.08 ± 0.04 at 15 °C, 1.31 ± 0.04 at 27 °C, and 1.42 ± 0.04 at 48 °C. One has to note that the χ_{eff} values obtained from the swelling process and from the drying process at the same temperature differ from each other. Because the χ_{eff} parameter is extracted by analyzing the kinetic swelling and drying processes, it refers either to water uptake (swelling) or to water release (drying). Hence, the dynamic processes have an impact on the χ_{eff} values, and therefore, we compare them with each other only within the respective dynamic process.

Furthermore, the χ_{eff} parameter excludes interactions between the substrate and the DBC, and it cannot be seen as an absolute Flory−Huggins parameter under particular ambient conditions. Hence, the focus lays rather on the trend than on the absolute of the χ_{eff} values.

The decreasing hydrophilicity upon temperature increase is already seen for the swelling kinetics. Hence, even though the DBC thin film shows at 27 °C a hydrophilicity, which lies in between the hydrophilicities at 15 and 48 °C, the release of water out of the film and the collapse of the DBC thin film are the fastest. During the swelling cycles, the water uptake at 27 °C takes roughly the same time as at 48 °C, although the DBC thin film is more hydrophilic at 27 °C, which usually implies longer diffusion pathways and therefore a prolonged water uptake. During the drying cycles, this effect is even more pronounced. It seems that the temperature of 27 °C represents optimum conditions for achieving fast water uptake and release. One possible explanation for this unexpected behavior could be a changing thin-film morphology dependent on the ambient temperature, as was shown in our previous work.[64] Diffusion pathways are shorter at 27 °C than at 15° because at 27 °C, the PNIPMAM cylinders within the PSPP matrix are partly collapsed, as is concluded from the static ToF-NR results (cf. Figures 2 and 3).

Assuming that water is absorbed into and released from the thin film via the hydrophilic parts of the DBC, the thin film at 27 °C bears better conditions for water uptake and release than at 48 °C. Here, the PNIPMAM block is more collapsed than at 27 °C, while the hydrophilicity of the PSPP block does not change with temperature. Hence, the temperature of 27 °C might provide balanced conditions between short diffusion pathways and a sufficient hydrophilic state, to achieve fast water uptake and release. It is noteworthy that similar to the swelling cycles, τ values differ at all temperatures, dependent on whether they are extracted from the evolution of the swelling ratio d/d_{ini} or from the water content Φ. During all drying cycles, the film thickness decreases faster than water is released from the DBC thin film, which is an inversion of the behavior from the swelling processes. During swelling, the film thickness increases more slowly than the water uptake. Thus, during the drying processes, the water release takes longer than the decrease in film thickness because of water that is released from the voids within the films. Hence, the water content still decreases, but the film thickness remains unaffected. At the end of film drying, some

residual water is still present inside the thin film, even though the RH is decreased to 0%, whereas the swelling ratio d/d_{ini} returns to roughly its initial value (also, see Figure 2).

3.3. Polymer−Water Interactions. In order to gain a more detailed insight into the behavior of D_2O, H_2O, and the characteristic SO_3^- group at the end of the PSPP side chain upon the swelling processes on the nanoscale, FTIR measurements are performed in situ during the swelling. Three swelling cycles at each temperature, 15, 27, and 48 °C, are studied. Figure 6 shows exemplarily the FTIR spectrum of the first swelling cycle at 15 °C over the wavenumber range of 600−4000 cm^{-1}. All FTIR spectra, for three swelling cycles at 15, 27, and 48 °C, are shown in Figure S4 in the Supporting Information.

The two very prominent absorption peaks appearing at ca. 2500 and 3400 cm^{-1} can be assigned to the O−D and O−H stretching vibrations, respectively. These broad peaks consist of several sub-bands, which correspond to various types of water molecules. These include those that are bound by hydrogen bonds to the polymer chains as well as those that move freely within the thin film.[73,74] At a wavenumber of around 1040 cm^{-1}, a very sharp peak arises, which represents the asymmetric S−O stretching vibration of the SO_3^- group. In our recent work, the hydration shell around this group was found to be the first one that builds up during a swelling process before the remaining polymer chains are hydrated.[35,64] The three smaller peaks between the prominent O−D and O−H stretching vibrations result from the symmetric (2886 cm^{-1}) and asymmetric (2974 cm^{-1}) C−H stretching vibrations of the CH3 groups and the asymmetric C−H stretching vibration (2938 cm^{-1}) of the CH2 groups. These groups remain unaffected by the swelling processes. Thus, all FTIR spectra are normalized to these C−H stretching vibrations to eliminate the effect of different thin-film thicknesses.

The normalized peak areas of the O−D and O−H stretching vibrations indicate the amount of O−H (H_2O, HDO) and O−D (D_2O, HDO) water species in the thin films. Furthermore, the hydration of the polymer chain during the swelling cycles is identified from the peak position of

the asymmetric S−O stretching vibration, which is sensitive to the chemicalenvironment. Figure 7 shows the evolution of the resulting normalized peak areas of the O−D (top row) and O−H (center row) stretching vibrations and the peak shift of the asymmetric S−O stretching vibration (bottom row) during the three swelling cycles at 15, 27, and 48 °C together with the swelling model fits (eqs S1−S4). A stacked representation of the data together with the fits is shown in the Supporting Information (Figure S5).

The trend of a decreasing hydrophilicity with increasing temperature observed in the ToF-NR investigations is also visible in the FTIR data because the normalized area of the O−D stretching vibration, and accordingly the number of water molecules present, decreases with increasing temperature. However, the trend is not as pronounced as that in the ToFNR experiments. Furthermore, we observe that within the three swelling cycles for each temperature, the area of the O−D stretching vibration reaches a plateau value at roughly the same normalized area. This differs profoundly from the results of the ToF-NR experiments, where the first swelling cycle reaches a lower water content Φ than the second and third swelling cycles. This underlines the differences in the probed information. Although ToF-NR probes mesoscopic parameters such as film thickness and water content, FTIR obtains information about the behavior of water molecules and characteristic groups of the DBC on the nanoscale. Moreover, in the first swelling cycles at 15 and 27 °C, the O−D stretching vibration needs a longer time to reach an equilibrium state. This hints toward changes in the polymer chain conformation, already discussed above, which leads to faster diffusion of water molecules and water uptake during the second and third swelling cycles.

Because the extracted parameters depend on the water content within the film, the swelling model that was already introduced for fitting the water content Φ determined with ToF-NR is also applied to the analysis of the FTIR data. All extracted χeff and τ values are listed in Table S4 in the Supporting Information. $\chi_{eff}(\mathrm{O-D})$ values decrease with increasing temperature, indicating a lower hydrophilicity at higher temperatures (0.51 ± 0.03 at 15 °C, 1.02 ± 0.04 at 27 °C, and 1.22

± 0.05 at 48 °C). Because of shorter diffusion pathways, $\tau(\mathrm{O-D})$ values decrease with increasing temperature [(3.1 ± 0.2) d at 15 °C, (1.8 ± 0.2) d at 27 °C, and (0.5 ± 0.1) d at 48 °C]. These values are in good agreement with the findings from ToF-NR measurements. At 15 and 27 °C, the first swelling cycle is the longest [(3.1 ± 0.2) d at 15 °C and (1.8 ± 0.2) d 27 °C], while the second and third swelling cycles are shorter [(2.7 ± 0.1) and (2.8 ± 0.1) d at 15 °C and (1.3 ± 0.1) and at 27 °C, respectively]. This supports the assumption of faster water molecule diffusion because of the changed polymer chain conformation during the second and third swelling cycles. Furthermore, the O−D stretching vibration is detected already before the second and third swelling cycles at 15 and 27 °C are started. This indicates an exchange of initially incorporated H_2O with D_2O molecules as well as partial polymer chain deuteration during the first swelling cycle. Again, these findings are in good agreement with the ToF-NR results. However, at 48 °C, we find a different behavior. Here, the $\tau(\mathrm{O-D})$ values for all three swelling cycles amount to (0.5 ± 0.1) d. Apparently, the water uptake is very limited, and the diffusion pathways are very short, such that no difference between the first and the following two swelling cycles can be seen. Also, the O−D offset before the second and third swelling cycles is much less pronounced as compared to the swelling cycles at 15 and 27 °C, indicating a less H_2O/D_2O exchange and a lower extent of polymer chain deuteration.

The evolution of the O−H stretching vibration during the three swelling cycles differs notably at 15 and 27 °C. During the first swelling cycle, the O−H stretching vibration is already detected at $t = 0$, corresponding to H_2O molecules present within the as-prepared film. An initial increase in absorption is observed at $t \leq 1$ d, attaining a maximum value. Afterward, the band area decreases somewhat, reaching a plateau after approximately 3.5 d. The increase can be explained by the reversed deuteration of the polymer chains' amide groups. Thereby, HDO molecules are generated, which also show an O−H stretching vibration. The area of the O−H stretching vibration indicative of its relative content within the film gradually decreases until the swelling process

eventually reaches an equilibrium state. Thus, with more D_2O molecules diffusing in the DBC thin film, HDO molecules are increasingly pushed out. At the beginning of the second swelling cycle, the absorbance of the O−H stretching vibration is decreased and only increases slightly before reaching a plateau value. Hence, less H_2O/HDO is present in the film at the start of the second cycle as compared to the first swelling cycle. Furthermore, the rate of deuteration is slower than that during the first swelling cycle. These observations are even more prominent in the third swelling cycle. No more H_2O/HDO molecules are present before the third swelling cycle starts, and deuteration is even slower than in the two previous swelling cycles. Still, even though the deuteration of the polymer chain is slower, it reaches the same plateau in the equilibrium state. Although the evolution of the O−H stretching vibration is a result of two opposing effects, namely, the deuteration of the secondary amide groups in the polymer and the displacement of H_2O and HDO molecules by D_2O, both kinetics are controlled by the diffusion process of D_2O molecules into the DBC thin film. Therefore, the swelling model can be applied. $\chi_{eff}(\mathrm{O-H})$ values follow the same trend as $\chi_{eff}(\mathrm{O-D})$ values. They increase with increasing temperature, again indicating a higher hydrophobicity at higher temperatures: 0.45 ± 0.02 at 15 °C, 0.95 ± 0.03 at 27 °C, and 1.13 ± 0.04 at 48 °C. However, the values of $\chi_{eff}(\mathrm{O-H})$ are slightly lower than $\chi_{eff}(\mathrm{O-D})$ values at the corresponding temperatures. This hints toward a higher affinity of the polymer to H2O than to D_2O, in agreement with previous reports.35 Also $\tau(\mathrm{O-H})$ values follow the same trend as observed for $\tau(\mathrm{O-D})$ values. With increasing temperature, the intensity of the O−H stretching vibration reaches the equilibrium value faster and $\tau(\mathrm{O-H})$ values decrease: (2.4 ± 0.2) d at 15 °C, (1.8 ± 0.2) d at 27 °C, and (0.1 ± 0.03) d at 48 °C. Furthermore, the values of $\tau(\mathrm{O-H})$ show that the first swelling cycle takes the longest time to reach an equilibrium state. This is ascribed to the entropically rather disadvantageous chain conformation regarding water uptake, as compared to the ones present in the second and third swelling cycles, which slows down the

diffusion rate. In addition, the exchange of H_2O and HDO by D_2O is expected to occur mainly during the first swelling cycle because more H_2O molecules are present within the film, as compared to the second and third swelling cycles. Moreover, the amide groups of the polymer chain are completely hydrogenated, which results in a higher deuteration rate and eventually leads to a higher amount of HDO molecules. Hence, the second and third swelling cycles yield smaller $\tau(\mathrm{O-H})$ values, which are in agreement with the opposed evolution of the $\tau(\mathrm{O-D})$ values. The swelling cycles at 48 °C, again, behave differently as the swelling model yields the same $\tau(\mathrm{O-H})$ value for all three swelling cycles (0.10 ± 0.03 d), and all three consecutive cycles exhibit a rapid but small increase in O−H stretching vibration intensity before reaching a plateau value. This behavior indicates a very fast but very low deuteration rate during every swelling cycle. Furthermore, the few HDO molecules that remain within the film after the first swelling cycle continue to stay. During the second and third swelling cycles, a slight decrease in absorption is monitored. Because of a low but constant deuteration process, more and more HDO molecules are generated over the first and second swelling cycles, which eventually lead to a minor HDO/D_2O exchange. Thus, the water uptake is very low, such that deuteration effects become negligible.

While the regions around 2500 and 3400 cm^{-1} directly reflect the overall fate of the water molecules present in the films during the swelling and shrinking cycles (Figure 7, upper two rows), the band at about 1040 cm^{-1} indicates the local interaction of specific polymer segments, namely, the anionic sulfonate moieties, with water during the exchange processes (Figure 7, the lower row). As a function of its hydration, the asymmetric S−O stretching vibration can shift to higher or lower wavenumbers, while its intensity remains virtually unchanged. For the swelling cycles at all temperatures, we observe a shift to higher wavenumbers, for which the swelling cycles at 15 °C provoke the strongest shift and the swelling cycles at 48 °C provoke the smallest shift. These differences are less pronounced than the ones observed for the O−D or O−H stretching vibration. Also, the changes of the S−O stretching vibration occur significantly faster than the ones of the

O−D or O−H stretching vibration. From previous work, we know that the hydration shell builds up around the SO_3^- group before the remaining polymer chain is hydrated.[35,64] The results indicate a similar behavior here. Although the water uptake decreases with increasing temperature, the shift in wavenumber of the S−O stretching vibration is almost the same at any of the three temperatures. Hence, the hydration shell around the SO_3^- group is similar at all temperatures. This conclusion is supported by applying the swelling model to the data. The evolution of the S−O stretching vibration exhibits by far the lowest $\chi_{eff}(\mathrm{S-O})$ and $\tau(\mathrm{S-O})$ values: 0.31 ± 0.03 and (0.80 ± 0.1) d at 15 °C, 0.73 ± 0.05 and (0.50 ± 0.1) d at 27 °C, and 0.98 ± 0.05 and (0.40 ± 0.1) d at 48 °C, respectively. Although the extent of the final peak shift is similar at all temperatures, a faster hydration of the SO_3^- group upon increasing temperature is observed because of shorter diffusion pathways and less favorable polymer−water interactions. Thus, the lower hydrophobicity of the polymer at higher temperatures has an effect on how fast but not on how strong the SO_3^- group is hydrated. This is in good agreement with the trend observed for the O−D stretching vibration.

Thus, *in situ* FTIR experiments reveal the complex interplay between different water species upon a swelling cycle and showed how deuteration of functional groups within the polymers and exchange processes are altered within consecutive swelling cycles.

4. Conclusions

In the present work, we investigate the cyclic water swelling−deswelling of a doubly thermoresponsive DBC thin film. The DBC consists of a large zwitterionic PSB and a considerably smaller nonionic PNIPMAM block, showing a UCST-type transition and a LCST-type transition, respectively, in aqueous solution. The DBC thin film is subjected to three swelling and drying cycles at three characteristic temperatures, 15, 27, and 48 °C, which cover the relevant regimes of the DBC known from the aqueous solution phase diagram. Both the swelling and drying processes are induced by changing the ambient RH. Upon swelling and drying, mesoscopic parameters such as film thickness and water content are modulated, which are followed in situ by ToF-NR.

Additionally, FTIR spectroscopy is applied during the swelling processes to obtain information about polymer−water interactions with increasing RH. A swelling model that takes into account the diffusion of water molecules into the thin film when the ambient RH changes is used to analyze quantitatively the measured data.

At the highest temperature studied, 48 °C, the DBC thin film exhibits the lowest swelling ratio d/d_{ini} and water content Φ within the film. This trend was unexpected because from the phase behavior of its aqueous solution, we would assume the lowest hydrophilicity at 15 °C (when the large polyzwitterion block is not water-soluble), an intermediate hydrophilicity at 48 °C (when the small nonionic block is not water-soluble), and the highest hydrophilicity at 27 °C (when both blocks are water-soluble). These observations can be explained by a strong shift of the respective transition temperatures CP_{UCST} and CP_{LCST} because of the thin-film geometry. While the polymer becomes less hydrophilic, the water uptake becomes faster because of reduced diffusion pathways and unfavorable polymer−water interactions. Noteworthily, the swelling kinetics at 27 and 48 °C occur on almost the same timescale, even though the DBC thin film shows a significantly lower hydrophilicity at 48 °C. A similar trend is observed during the drying kinetics. With a decreasing hydrophilicity, faster water release is expected at higher temperatures. However, the fastest water release is observed at 27 °C, which indicates that at this particular temperature, the thin-film morphology is optimal for fast water uptake and release. Apparently, this is due to an advantageous superposition of shortened diffusion pathways as compared to the thin film at 15 °C, and a higher hydrophilicity as compared to the thin film at 48 °C.

On a molecular level, the O−H and O−D stretching vibrations can be clearly distinguished in the FTIR spectra so that the complex interplay between different water species (H_2O, HDO, and D_2O) is revealed. During the first swelling cycles at 15 and 27 °C, the initially present H_2O molecules

within the film are substituted by D_2O. Furthermore, selective partial deuteration of the polymer chain is observed. Foremost, the acidic hydrogen atom in the amide group, which is present in

both polymer blocks, is exchanged by a deuterium atom. This leads to a third present water species, HDO, which is gradually expelled from the film, while more D_2O molecules diffuse into the film. During the second and third swelling cycles, less H_2O and HDO, respectively, are present, while the deuteration rate also slows down. Nonetheless, the O−H stretching vibration still reaches the same absorption values as in the cycles before.

The consecutive swelling cycles at 48 °C differ significantly from those at lower temperatures. Barely no HDO species is detected, which indicates a very little amount of HDO and therefore a very weak HDO/D_2O exchange as well. Apparently, the water uptake in general is reduced in a way that deuteration effects of the amide groups play a minor role. The analysis of the shift of the asymmetric S−O stretching vibration indicates that the hydration shell builds up rapidly around this group before the remaining polymer chain is hydrated. No significant differences in the hydration of the SO_3^- group at different temperatures could be detected. Accordingly, the overall swelling behavior of the DBC is affected by a change in hydrophilicity, without necessarily changing the hydration of particular groups within the macromolecules.

The presented results provide valuable insights into the repeated swelling and drying of a doubly thermoresponsive DBC thin film. The swelling behavior differs significantly from our expectations based on the DBC behavior in aqueous solution. Furthermore, it depends not only on the chosen temperature but is also altered in the course of three consecutive swelling cycles at constant temperature. This is attributed to the thin-film processing by spin coating that yields a nonequilibrated film structure. This study shows the complexity of such a thin-film system and simultaneously puts it into context to previous results on cyclic swelling of thermoresponsive thin films. Although a change in chain conformation during the first swelling cycle is found, neither an aging process nor a decreased water storage ability are observed. Thereby, the need of a fundamental understanding of the underlying mechanisms of such responsive materials in the thin-film geometry, also in the perspective of their possible uses, is stressed out.

Author Information

Corresponding Author: Peter Müller-Buschbaum − Lehrstuhl für Funktionelle Materialien, Physik Department and Heinz Maier-Leibnitz Zentrum (MLZ), Technische Universitat München, 85748 Garching, Germany; Phone: +49 89 289 12451; Email: muellerb@ph.tum.de; Fax: +49 89 289 12473

Author Contrinbutions

The manuscript was written through contributions of all authors. All authors have given approval to the final version of the manuscript.

Funding

The authors thank Deutsche Forschungsgemeinschaft (DFG) for financial support (PA 771/14-1, MU 1487/17-1, and LA 611/11-1), and L.P.K. and T.W. thank the BMBF project "Flexiprobe" (grant number 05K16WOA).

Notes

The authors declare no competing financial interest.

Acknowledgements

The Heinz Maier-Leibnitz Zentrum is acknowledged for beam time allocation and for providing excellent equipment

Figures and Schemes

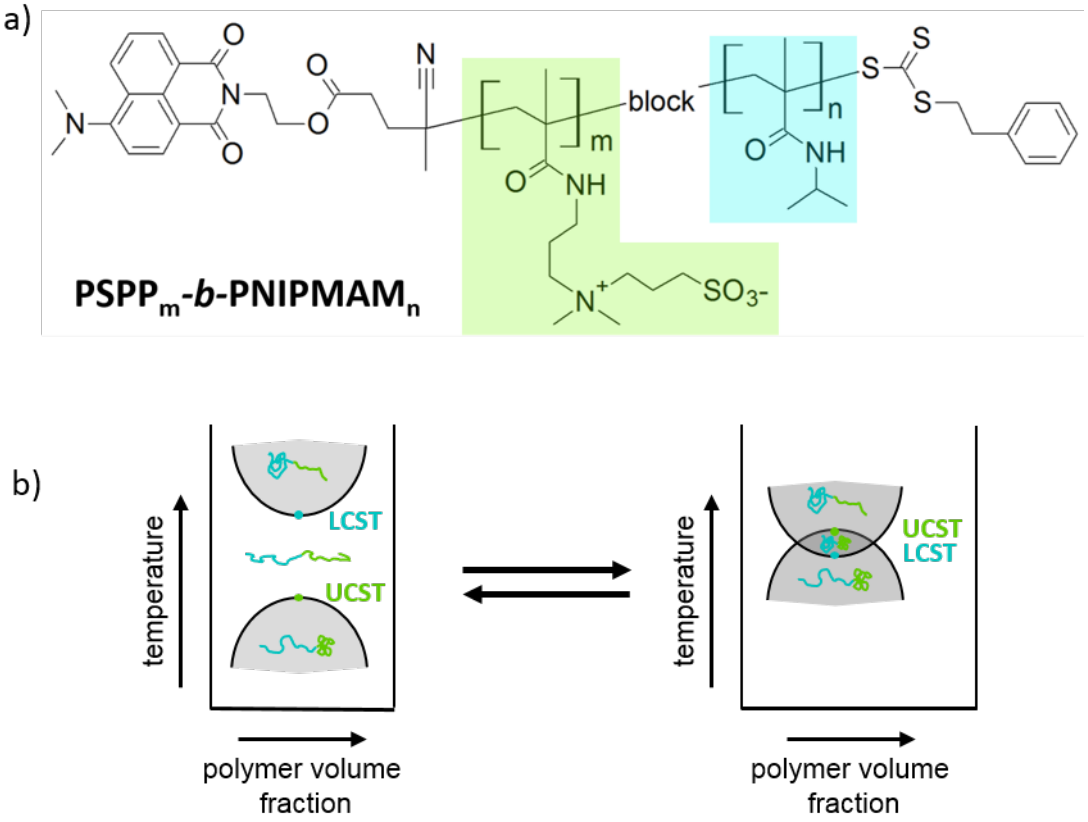

Figure 1: a) Chemical structure of the DBC under study, PSPP$_m$-*b*-PNIPMAM$_n$ (m = 500, n = 150). The PSPP block is colored in green, the PNIPMAM block is colored in blue. b) The 'schizophrenic' micellar self-assembly of a doubly thermo-responsive DBC is shown schematically. Interactions induced by the interfaces from the thin film geometry can change the relative positions of CP_{UCST} and CP_{LCST}.

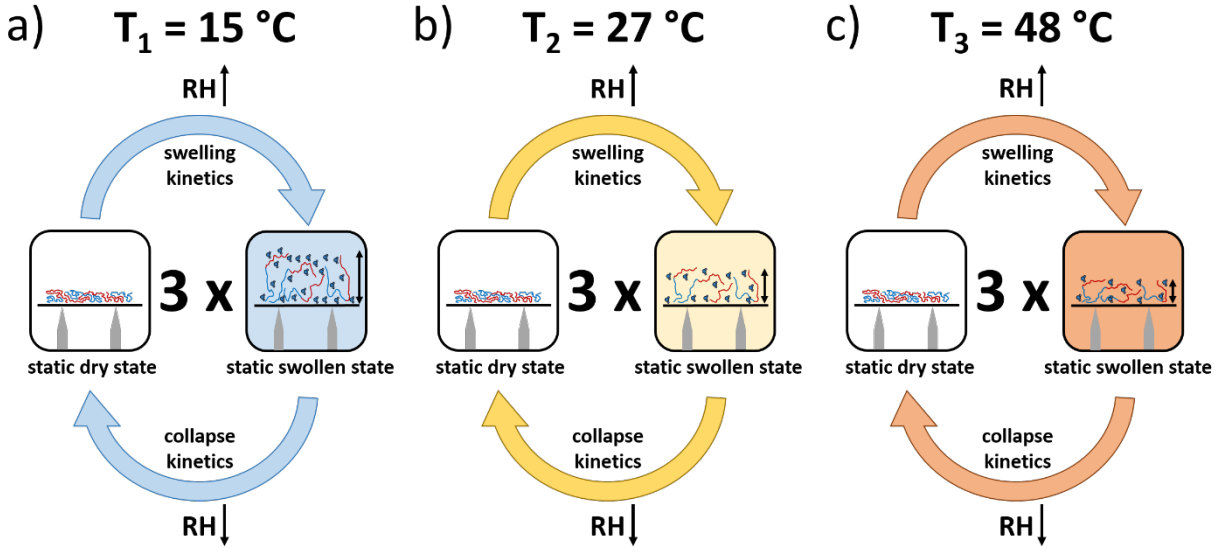

Scheme 1:.Schematic Overview of the Three Performed Experiments: Three Consecutive Cycles of D_2O Swelling and Drying Are Followed with ToF-NR In Situ at 15 (a), 27 (b), and 48 °C (c). The swelling process is induced by increasing and the collapse process by decreasing the RH. The characteristic temperatures were chosen to be: a) below both CP_{UCST} and CP_{LCST}, b) above the CP_{UCST} but below the CP_{LCST}, and (c) above both CP_{UCST} and CP_{LCST} of the DBC in aqueous solution.

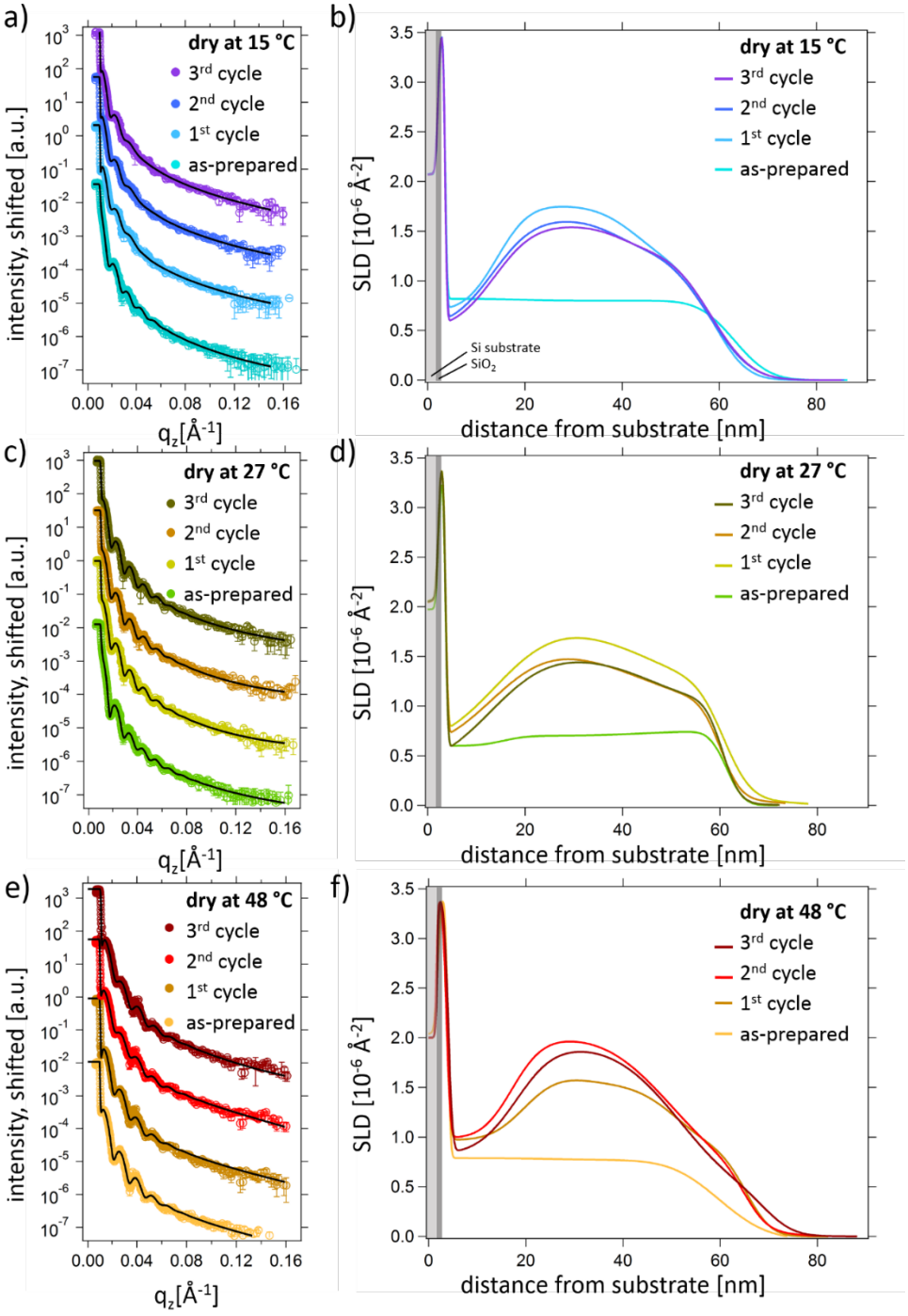

Figure 2: Static ToF-NR measurements of $PSPP_{500}$-*b*-$PNIPMAM_{150}$ films in its dry states during in total three swelling cycles at: a) 15 °C, c) 27 °C, and e) 48 °C, respectively. The curves are

shifted along the *y*-axis for clarity of the presentation. The cycle number increases from bottom (as-prepared) to top (third cycle). Best fits are achieved with a three-layer model (black lines). From the fits, the SLD profiles of the corresponding dry states at b) 15 °C, d) 27 °C, and f) 48 °C are obtained.

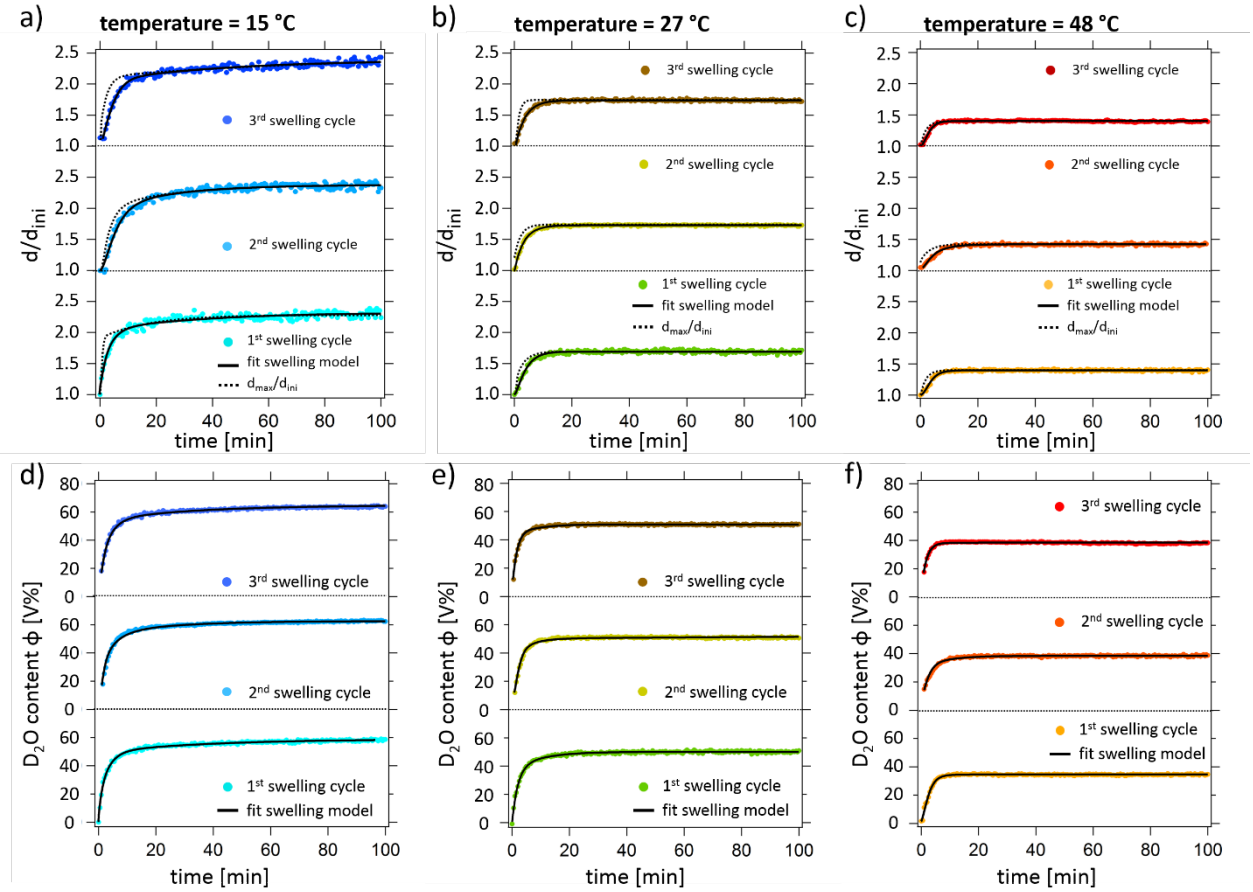

Figure 3: (a-c) Swelling ratio d/d_{ini} and (d-f) water content Φ as a function of time during three swelling cycles at (a and d) 15 °C, (b and e) 27 °C, and (c and f) 48 °C, respectively. The cycle number increases from bottom (first swelling cycle) to top (third swelling cycle). The curves are fitted with the swelling model as explained in the text (black line). In addition to the swelling ratio d/d_{ini}, the maximum swelling ratio $d_{\max}/d_{ini}$ is plotted (dashed black line in graphs a-c).

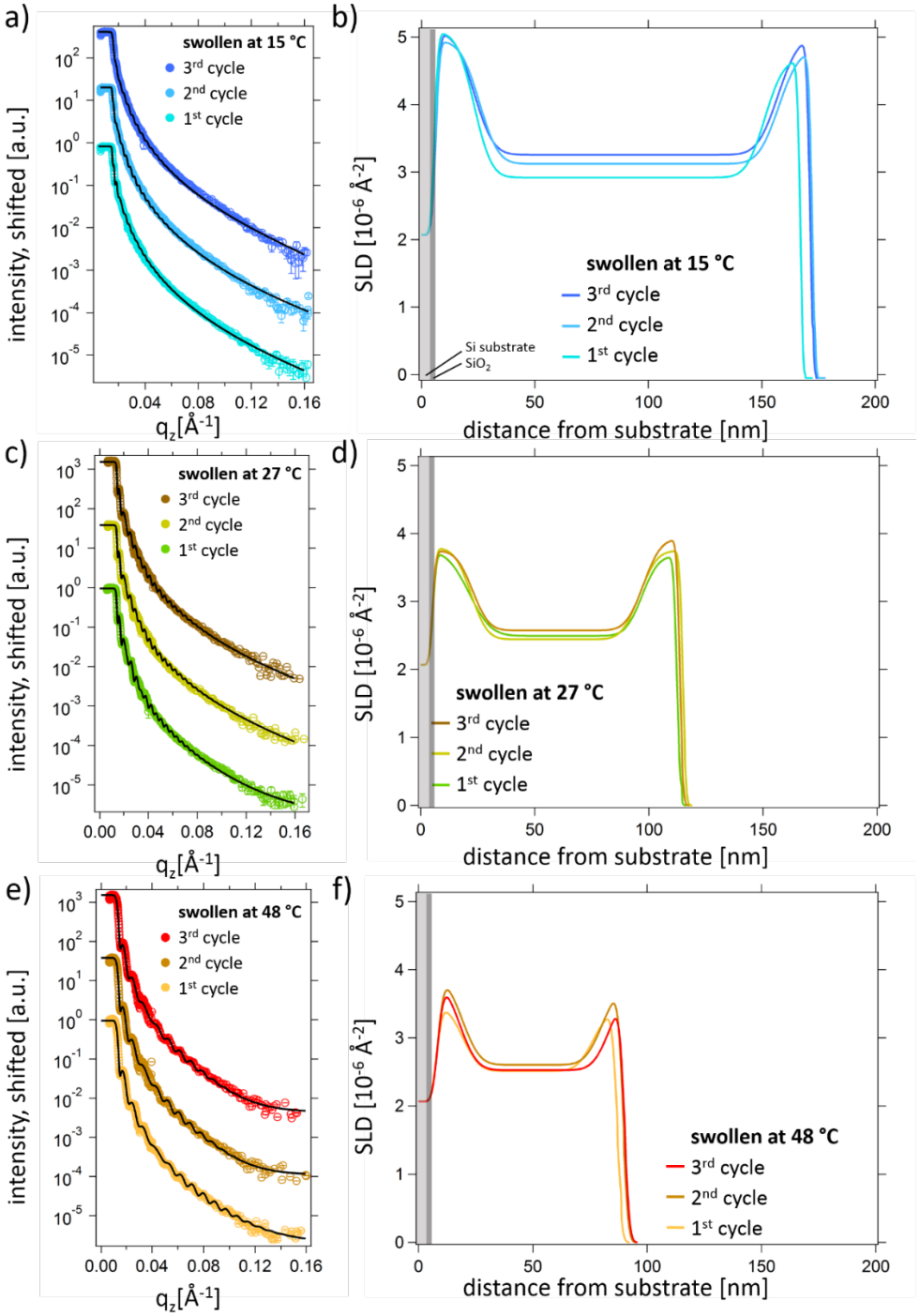

Figure 4: Static ToF-NR measurements of $PSPP_{500}$-*b*-$PNIPMAM_{150}$ films in its D_2O swollen states over in total three swelling cycles at (a) 15 °C, (c) 27 °C, and (d) 48 °C, respectively. The curves are shifted along the y axis for clarity of the presentation. The cycle number increases from bottom (after first swelling cycle) to top (after third swelling cycle). Best fits were achieved with a three-layer model. From the fits, the SLD profiles of the corresponding D_2O swollen states at (b) 15 °C, (d) 27 °C, and (f) 48 °C are obtained.

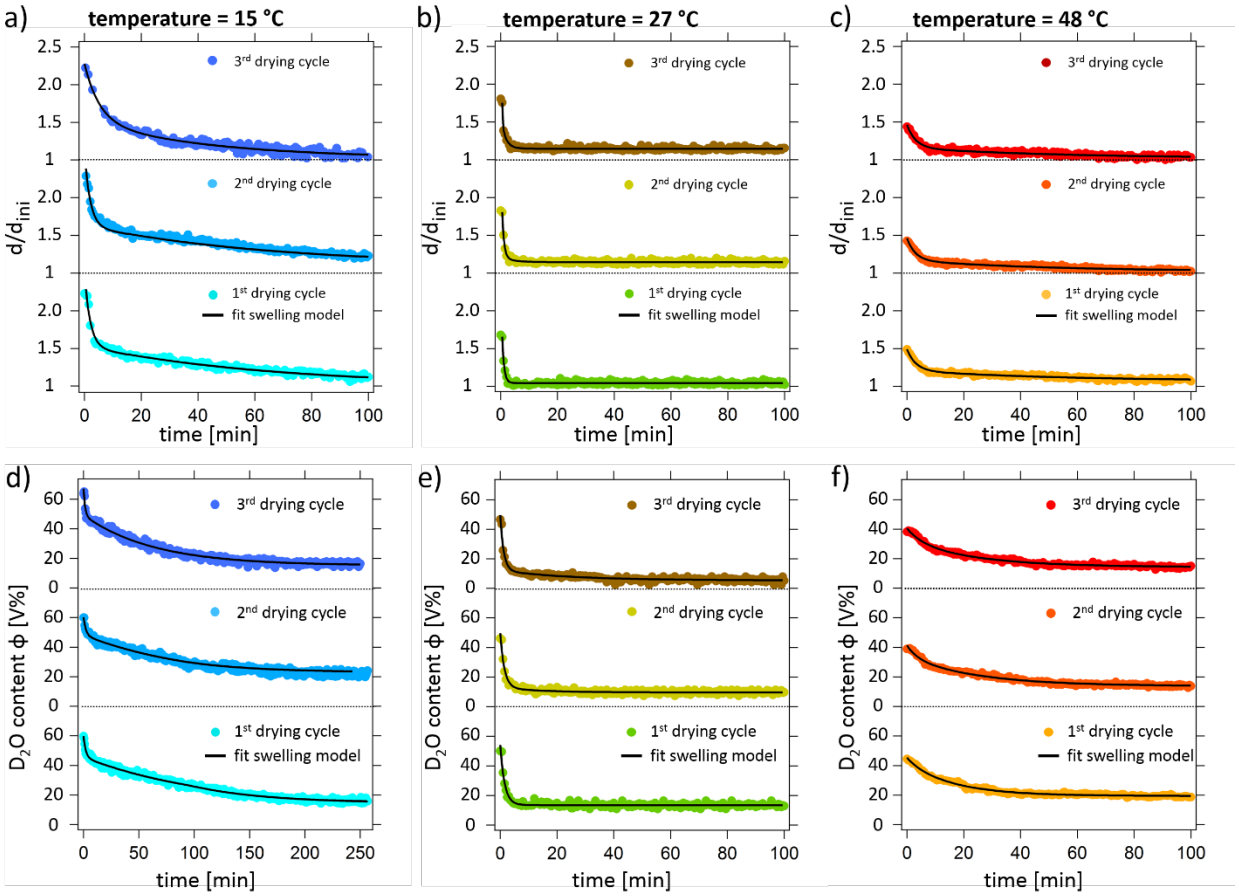

Figure 5: Swelling ratio d/d_{ini} (a-c) and water content Φ (d-f) as a function of time during collapsing cycles, which are induced by drying, at (a and d) 15 °C, (b and e) 27 °C, and (c and f) 48 °C, respectively. The cycle number increases from bottom (first drying cycle) to top (third drying cycle). The curves are fitted with the swelling model as explained in the text (black line).

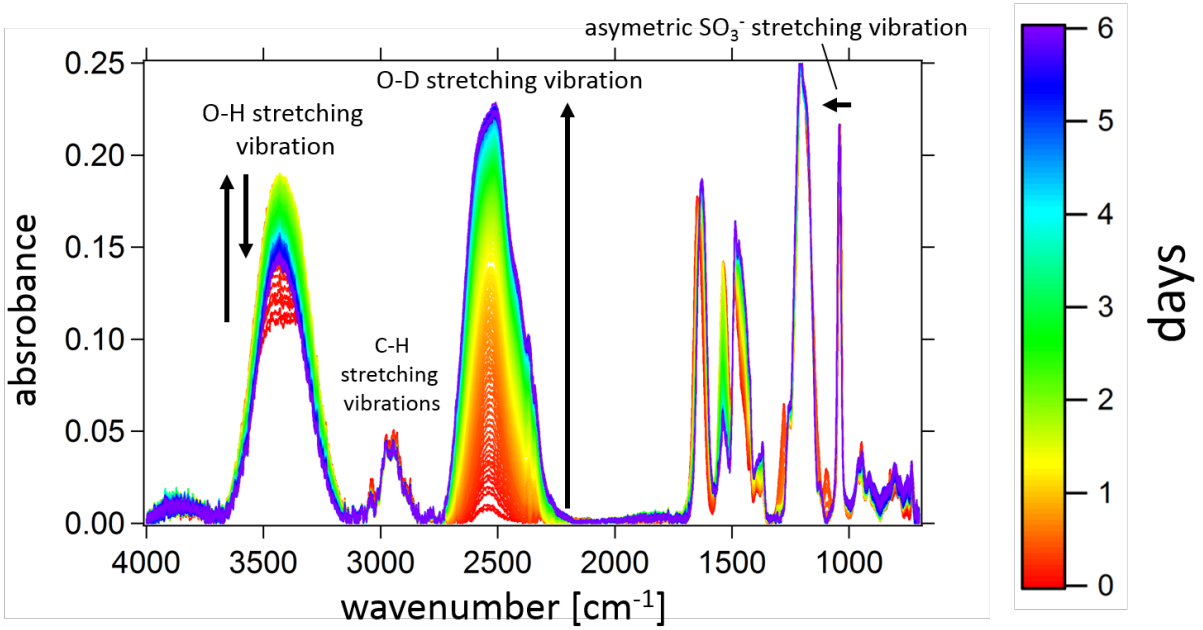

Figure 6: Exemplary FTIR spectrum of the first swelling cycle at 15 °C. The first measurement is colored in red ($t = 0$ d), whereas the last measurement is colored in purple ($t = 6$ d) as indicated by the color bar.

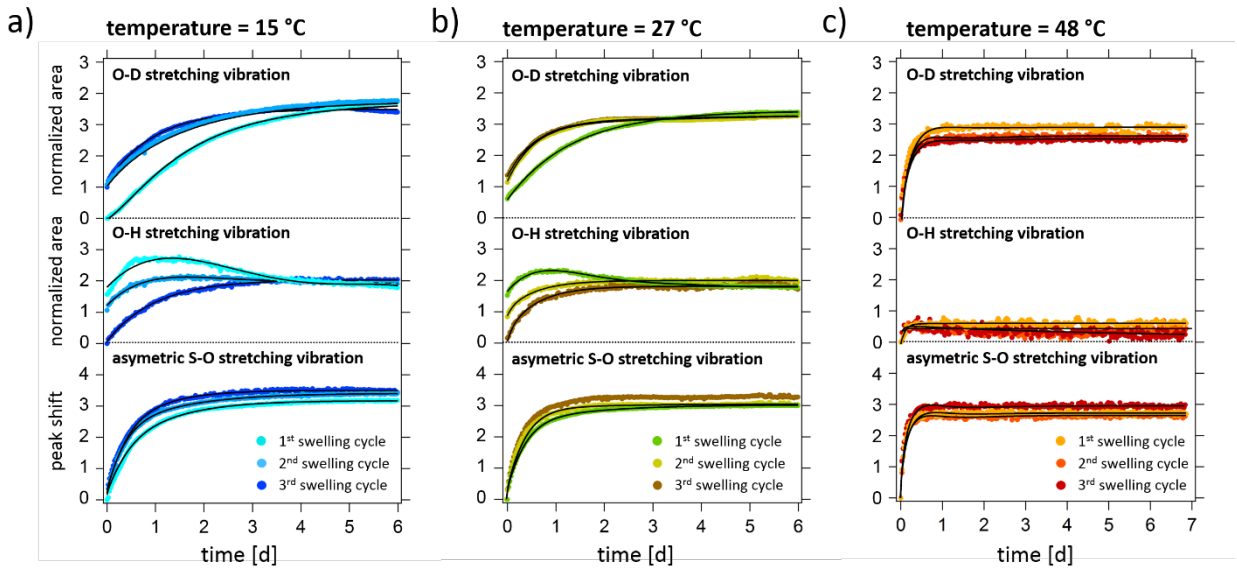

Figure 7: The normalized area of the O-D stretching vibration (top), the normalized area of the O-H stretching vibration (center) and the shift of the SO_3^- peak maximum (bottom) at (a) 15 °C, (b) 27 °C, and (c) 48 °C as extracted from the FTIR spectra. All curves are fitted with the swelling model based as explained in the main text (black line).

Tables

Table 1: Film thickness d (sum of all layers) and the SLD (averaged over all layers) of the $PSPP_{500}$-*b*-$PNIPMAM_{150}$ thin film from the fits shown in Figure 2 (dry states) and Figure 4 (swollen states).

	dry state		**swollen state**	
15 °C	**thickness [nm]**	**SLD 10^{-6}[Å^{-2}]**	**thickness [nm]**	**SLD 10^{-6}[Å^{-2}]**
as-prepared	63 ± 3	0.91 ± 0.02	---	---
first cycle	63 ± 2	1.37 ± 0.02	190 ± 4	3.55 ± 0.05
second cycle	62 ± 2	1.32 ± 0.03	194 ± 4	3.51 ± 0.05
third cycle	61 ± 2	1.31 ± 0.03	205 ± 4	3.48 ± 0.04

27 °C				
as-prepared	65 ± 3	0.85 ± 0.01	---	---
first cycle	65 ± 3	1.37 ± 0.03	110 ± 2	3.05 ± 0.04
second cycle	64 ± 4	1.32 ± 0.03	112 ± 2	2.96 ± 0.04
third cycle	65 ± 3	1.31 ± 0.02	111 ± 1	3.00 ± 0.03
48 °C				
as-prepared	60 ± 2	0.90 ± 0.02	---	---
first cycle	63 ± 2	1.25 ± 0.03	87 ± 2	2.75 ± 0.02
second cycle	63 ± 3	1.52 ± 0.04	87 ± 2	2.75 ± 0.01
third cycle	61 ± 2	1.38 ± 0.03	87 ± 1	2.68 ± 0.02

References

1. Mirvakili, S. M.; Hunter, I. W. Artificial Muscles: Mechanisms, Applications, and Challenges. *Adv. Mater* **2018**, *30*, 1704407.
2. Ghosh, A.; Yoon, C.; Ongaro, F.; Scheggi, S.; Selaru, F. M.; Misra, S.; Gracias, D. H. Stimuli-Responsive Soft Untethered Grippers for Drug Delivery and Robotic Surgery. *Front. Mech. Eng.* **2017**, *3*, 73.
3. Richter A.; Paschew G.; Klatt S.; Lienig J.; Arndt K.-F.; Adler H.-J. P. Review on Hydrogel-based pH Sensors and Microsensors. *Sensors* **2008**, 561–581.
4. Hu, J.; Liu, S. Responsive Polymers for Detection and Sensing Applications: Current Status and Future Developments. *Macromolecules* **2010**, *43*, 8315–8330.
5. Buenger, D.; Topuz, F.; Groll, J. Hydrogels in Sensing Applications. *Prog. Polym. Sci.* **2012**, *37*, 1678–1719.
6. Stumpel, J. E.; Broer, D. J.; Schenning, A. P. H. J. Stimuli-Responsive Photonic Polymer Coatings. *Chem. Commun.* **2014**, *50*, 15839–15848.
7. Chen, W.; Ma, Y.; Pan, J.; Meng, Z.; Pan, G.; Sellergren, B. Molecularly Imprinted Polymers with Stimuli-Responsive Affinity: Progress and Perspectives. *Polymers* **2015**, *7*, 1689–1715.
8. Couturier, J.-P.; Sütterlin, M.; Laschewsky, A.; Hettrich, C.; Wischerhoff, E. Responsive Inverse Opal Hydrogels for the Sensing of Macromolecules. *Angew. Chem., Int. Ed.* **2015**, *54*, 6641–6644.
9. Culver, H. R.; Clegg, J. R.; Peppas, N. A. Analyte-Responsive Hydrogels: Intelligent Materials for Biosensing and Drug Delivery. *Acc. Chem. Res.* **2017**, *50*, 170–178.

10. Wei, M.; Gao, Y.; Li, X.; Serpe, M. J. Stimuli-Responsive Polymers and their Applications. *Polym. Chem.* **2017**, *8*, 127–143.
11. Wischerhoff, E.; Badi, N.; Laschewsky, A.; Lutz, J.-F. Smart Polymer Surfaces: Concepts and Applications in Biosciences. *Adv. Polym. Sci.* **2011**, 1–33.
12. Roy, D.; Brooks, W. L. A.; Sumerlin, B. S. New Directions in Thermoresponsive Polymers. *Chem. Soc. Rev.* **2013**, *42*, 7214–7243.
13. Nagase, K.; Okano, T. Thermoresponsive-Polymer-Based Materials for Temperature-Modulated Bioanalysis and Bioseparations. *J. Mater. Chem. B* **2016**, *4*, 6381–6397.
14. Esmaeilzadeh, P.; Groth, T. Switchable and Obedient Interfacial Properties That Grant New Biomedical Applications. *ACS Appl. Mater. Interfaces* **2019**, *11*, 25637–25653.
15. Blackman, L. D.; Gunatillake, P. A.; Cass, P.; Locock, K. E. S. An Introduction to Zwitterionic Polymer Behavior and Applications in Solution and at Surfaces. *Chem. Soc. Rev.* **2019**, *48*, 757–770.
16. Bhattacharya, S.; Sharma, D. K.; Saurabh, S.; De, S.; Sain, A.; Nandi, A.; Chowdhury, A. Plasticization of Poly(vinylpyrrolidone) Thin Films under Ambient Humidity: Insight from Single-Molecule Tracer Diffusion Dynamics. *J. Phys. Chem. B* **2013**, *117*, 7771–7782.
17. Graves-Abe, T.; Pschenitzka, F.; Jin, H. Z.; Bollman, B.; Sturm, J. C.; Register, R. A. Solvent-Enhanced Dye Diffusion in Polymer Thin Films for Polymer Light-Emitting Diode Application. *J. Appl. Phys.* **2004**, *96*, 7154–7163.
18. Wang, W.; Metwalli, E.; Perlich, J.; Papadakis, C. M.; Cubitt, R.; Müller-Buschbaum, P. Cyclic Switching of Water Storage in Thin Block Copolymer Films Containing Poly(N -isopropylacrylamide). *Macromolecules* **2009**, *42*, 9041–9051.
19. Shang, J.; Le, X.; Zhang, J.; Chen, T.; Theato, P. Trends in Polymeric Shape Memory Hydrogels and Hydrogel Actuators. *Polym. Chem.* **2019,** *10*, 1036−1055.
20. Kaneko, D.; Gong, J. P.; Osada, Y. Polymer Gels as Soft and Wet Chemomechanical ystems – An A Approach to Artificial Muscles. *J. Mater. Chem.* **2002,** *12*, 2169−2177.
21. Lei, Z.; Wang, Q.; Wu, P. A Multifunctional Skin-like Sensor Based on a 3D Printed Thermo-responsive *Hydrogel. Mater. Horiz.* **2017,** *4*, 694−700.
22. Shi, P.; Amb, C. M.; Dyer, A. L.; Reynolds, J. R. Fast Switching Water Processable Electrochromic Polymers. *ACS Appl. Mater. Interfaces* **2012**, *4*, 6512–6521.
23. Xu, P.; Murtaza, I.; Shi, J.; Zhu, M.; He, Y.; Yu, H.; Goto, O.; Meng, H. Highly Transmissive Blue Electrochromic Polymers Based on Thieno[3,2-b]thiophene. *Polym. Chem.* **2016**, *7*, 5351–5356.
24. Buchberger, A.; Peterka, S.; Coclite, A. M.; Bergmann, A. Fast Optical Humidity Sensor Based on Hydrogel Thin Film Expansion for Harsh Environment. *Sensors* **2019**, *19*, 999
25. Tang, H.; Zhang, B.; Wu, P. On the Two-Step Phase Transition Behavior of the Poly(N-isopropylacrylamide) (PNIPAM) Brush: Different Zones with Different Orders. *Soft matter* **2014**, *10*, 7278–7284.
26. Bischofberger, I.; Trappe, V. New Aspects in the Phase Behaviour of Poly-N-isopropylacrylamide: Systematic Temperature Dependent Shrinking of PNiPAM Assemblies well Beyond the LCST. *Sci. Rep.* **2015**, *5*, 15520.
27. Micciulla, S.; Soltwedel, O.; Löhmann, O.; Klitzing, R. von. Temperature Responsive Behavior of Polymer Brush/Polyelectrolyte Multilayer Composites. *Soft matter* **2016**, *12*, 1176–1183.
28. Janes, D. W.; Chandrasekar, V.; Woolford, S. E.; Ludwig, K. B. Predicting the Effects of Composition, Molecular Size and Shape, Plasticization, and Swelling on the Diffusion of Aromatic Additives in Block Copolymers. *Macromolecules* **2017**, *50*, 6137–6148.
29. Vergadou, N.; Theodorou, D. N. Molecular Modeling Investigations of Sorption and Diffusion of Small Molecules in Glassy Polymers. *Membranes* **2019**, *9*, 98.
30. Hellweg, T.; Dewhurst, C. D.; Eimer, W.; Kratz, K. PNIPAM-co-Polystyrene Core−Shell Microgels. *Langmuir* **2004**, *20*, 4330–4335.

31. París, R.; Quijada-Garrido, I.; García, O.; Liras, M. BODIPY-Conjugated Thermo-Sensitive Fluorescent Polymers Based On 2-(2-methoxyethoxy)ethyl methacrylate. *Macromolecules* **2011**, *44*, 80–86.
32. Gaulding, J. C.; Smith, M. H.; Hyatt, J. S.; Fernandez-Nieves, A.; Lyon, L. A. Reversible Inter- and Intra-Microgel Cross-Linking using Disulfides. *Macromolecules* **2012**, *45*, 39–45.
33. Klouda, L. Thermoresponsive Hydrogels in Biomedical Applications: A Seven-Year Update. *Eur. J. Pharm.* **2015**, *97*, 338–349.
34. Matsumoto, K.; Sakikawa, N.; Miyata, T. Thermo-Responsive Gels that Absorb Moisture and Ooze Water. *Nat. Commun.* **2018**, *9*, 2315.
35. Kreuzer, L. P.; Widmann, T.; Hohn, N.; Wang, K.; Bießmann, L.; Peis, L.; Moulin, J.-F.; Hildebrand, V.; Laschewsky, A.; Papadakis, C. M.; Müller-Buschbaum, P. Swelling and Exchange Behavior of Poly(sulfobetaine)-Based Block Copolymer Thin Films. *Macromolecules* **2019**, *52*, 3486–3498.
36. Jung, F. A.; Panteli, P. A.; Ko, C.-H.; Kang, J.-J.; Barnsley, L. C.; Tsitsilianis, C.; Patrickios, C. S.; Papadakis, C. M. Structural Properties of Micelles Formed by Telechelic Pentablock Quaterpolymers with pH-Responsive Midblocks and Thermoresponsive End Blocks in Aqueous Solution. *Macromolecules* **2019,** *52*, 9746−9758.
37. Hruby, M.; Štěpánek, P.; Pánek, J.; Papadakis, C. M. Crosstalk Between Responsivities to Various Stimuli in Multiresponsive Polymers: Change in Polymer Chain and External Environment Polarity as the Key Factor. *Colloid Polym. Sci.* **2019,** *297*, 1383−1401.
38. Schulz, D., N.; Pfeiffer, D., G.; Agarwal P., K.; Laraee J.; Kaladas J., J.; Soni L; Handwerker B.; Garner R., T. Phase Behaviour and Solution Properties of Sulphobetaine Polymers. *Polymer* **1986**, 1734–1742.
39. Hildebrand, V.; Laschewsky, A.; Zehm, D. On the Hydrophilicity of Polyzwitterion Poly(N,N-dimethyl-N-(3-(methacrylamido)propyl)ammoniopropane sulfonate) in Water, Deuterated Water, and Aqueous Salt Solutions. *J. Biomater. Sci., Polym. Ed.* **2014**, *25*, 1602–1618.
40. Niebuur, B.-J.; Puchmayr, J.; Herold, C.; Kreuzer, L. P.; Hildebrand, V.; Müller-Buschbaum, P.; Laschewsky, A.; Papadakis, C. M. Polysulfobetaines in Aqueous Solution and in Thin Film Geometry. *Materials* **2018**, *11*.
41. Wang, N.; Seymour, B. T.; Lewoczko, E. M.; Kent, E. W.; Chen, M.-L.; Wang, J.-H.; Zhao, B. Zwitterionic Poly(sulfobetaine methacrylate)s in Water: from Upper Critical Solution Temperature (UCST) to Lower Critical Solution Temperature (LCST) with Increasing Length of one Alkyl Substituent on the Nitrogen Atom. *Polym. Chem.* **2018**, *9*, 5257–5261.
42. Monroy Soto, V. M.; Galin, J. C. Poly(sulphopropylbetaines): 2. Dilute Solution Properties. *Polymer* **1984**, 254–262.
43. NNiskanen, J.; Tenhu, H. How to manipulate the upper critical solution temperature (UCST)? *Polym. Chem.* **2017,** *8*, 220−232.
44. Seuring, J.; Agarwal, S. Polymers with upper critical solution temperature in aqueous solution. *Macromol. Rapid Commun.* **2012,** *33*, 1898−1920.
45. Bohrisch, J.; Schimmel, T.; Engelhardt, H.; Jaeger, W. Charge Interaction of Synthetic Polycarboxybetaines in Bulk and Solution. *Macromolecules* **2002,** *35*, 4143−4149.
46. Bonte, N.; Laschewsky, A. Zwitterionic Polymers with Carbobetaine Moieties. *Polymer* **1996**, *37*, 2011–2019.
47. Favresse, P.; Laschewsky, A. Synthesis and Investigation of New Amphiphilic Poly(carbobetaine)s Made from Diallylammonium Monomers. *Polymer* **2001**, *42*, 2755–2766.

48. Ishihara, K.; Mu, M.; Konno, T.; Inoue, Y.; Fukazawa, K. The unique hydration state of poly(2-methacryloyloxyethyl phosphorylcholine). *Journal of biomaterials science. Polymer edition* **2017,** *28*, 884−899.
49. Grainger, D. W. All Charged Up About Implanted Biomaterials. *Nat. Biotechnol.* **2013**, 507–509.
50. Shao, Q.; Jiang, S. Molecular Understanding and Design of Zwitterionic Materials. *Adv. Mater* **2015**, *27*, 15–26.
51. Sin, M.-C.; Chen, S.-H.; Chang, Y. Hemocompatibility of Zwitterionic Interfaces and Membranes. *Polym J* **2014**, *46*, 436–443.
52. Laschewsky, A.; Rosenhahn, A. Molecular Design of Zwitterionic Polymer Interfaces: Searching for the Difference. *Langmuir* **2019,** *35*, 1056−1071
53. Fujishige, S. Phase Transition of Aqueous Solutions of Poly(N-isopropylacrylamide) and Poly(N-isopropylmethacrylamide). *J. Phys. Chem.* **1989**, 3311–3313.
54. Tiktopulo. E. I.; Uversky, V. N.; Lushchik, V. B.; Klenin, S. I.; Bychkova, V. E.; Ptitsyn, O. B. 'Domain' Coil-Globule Transitions in Homopolymers. *Macromolecules* **1995**, 7519–7524.
55. Spěváček, J.; Dybal, J. Temperature-Induced Phase Separation and Hydration in Aqueous Polymer Solutions Studied by NMR and IR Spectroscopy: Comparison of Poly(N - vinylcaprolactam) and Acrylamide-Based Polymers. *Macromol. Symp.* **2014**, *336*, 39–46.
56. Bütün, V.; Liu, S.; Weaver, J.V.M.; Bories-Azeau, X.; Cai, Y.; Armes, S. P. A Brief Review of 'Schizophrenic' Block Copolymers. *React. Funct. Polym.* **2006**, *66*, 157–165.
57. Vishnevetskaya, N. S.; Hildebrand, V.; Niebuur, B.-J.; Grillo, I.; Filippov, S. K.; Laschewsky, A.; Müller-Buschbaum, P.; Papadakis, C. M. Aggregation Behavior of Doubly Thermoresponsive Polysulfobetaine- b -poly(N -isopropylacrylamide) Diblock Copolymers. *Macromolecules* **2016**, *49*, 6655–6668.
58. Vishnevetskaya, N. S.; Hildebrand, V.; Niebuur, B.-J.; Grillo, I.; Filippov, S. K.; Laschewsky, A.; Müller-Buschbaum, P.; Papadakis, C. M. "Schizophrenic" Micelles from Doubly Thermoresponsive Polysulfobetaine- b -poly(N -isopropylmethacrylamide) Diblock Copolymers. *Macromolecules* **2017**, *50*, 3985–3999.
59. Vishnevetskaya, N. S.; Hildebrand, V.; Dyakonova, M. A.; Niebuur, B.-J.; Kyriakos, K.; Raftopoulos, K. N.; Di, Z.; Müller-Buschbaum, P.; Laschewsky, A.; Papadakis, C. M. Dual Orthogonal Switching of the "Schizophrenic" Self-Assembly of Diblock Copolymers. *Macromolecules* **2018**, *51*, 2604–2614.
60. Papadakis, C. M.; Müller-Buschbaum, P.; Laschewsky, A. Switch It Inside-Out: "Schizophrenic" Behavior of All Thermoresponsive UCST-LCST Diblock Copolymers. *Langmuir* **2019**, *35*, 9660–9676.
61. Makinen, L.; Varadharajan, D.; Tenhu, H.; Hietala, S. Triple Hydrophilic UCST−LCST Block Copolymers. *Macromolecules* **2016,** *49*, 986−993.
62. Hildebrand, V.; Heydenreich, M.; Laschewsky, A.; Möller, H. M.; Müller-Buschbaum, P.; Papadakis, C. M.; Schanzenbach, D.; Wischerhoff, E. "Schizophrenic" Self-Assembly of Dual Thermoresponsive Block Copolymers Bearing a Zwitterionic and a Non-Ionic Hydrophilic Block. *Polymer* **2017**, *122*, 347–357.
63. Hildebrand, V.; Laschewsky, A.; Päch, M.; Müller-Buschbaum, P.; Papadakis, C. M. Effect of the Zwitterion Structure on the Thermo-Responsive Behaviour of Poly(sulfobetaine methacrylates). *Polym. Chem.* **2017**, *8*, 310–322.
64. Kreuzer, L. P.; Widmann, T.; Bießmann, L.; Hohn, N.; Pantle, J.; Märkl, R.; Moulin, J.-F.; Hildebrand, V.; Laschewsky, A.; Papadakis, C. M.; Müller-Buschbaum, P. Phase Transition Kinetics of Doubly Thermoresponsive Poly(sulfobetaine)-Based Diblock Copolymer Thin Films. *Macromolecules* **2020**, *53*, 2841–2855.
65. Widmann, T.; Kreuzer, L. P.; Hohn, N.; Bießmann, L.; Wang, K.; Rinner, S.; Moulin, J.-F.; Schmid, A. J.; Hannappel, Y.; Wrede, O.; Kühnhammer, M.; Hellweg, T.; Klitzing, R.

von; Müller-Buschbaum, P. Hydration and Solvent Exchange Induced Swelling and De-Swelling of Homogeneous Poly(N-isopropylacrylamide) Microgel Thin Films. *Langmuir* **2019**.
66. Kampmann, R.; Haese-Seiller, M.; Kudryashov, V.; Deriglazov, V.; Tristl, M.; Daniel, C.; Toperverg, B.; Schreyer, A.; Sackmann, E. The Potential of the Horizontal Reflectometer REFSANS/FRM-II for Measuring Low Reflectivity and Diffuse Surface Scattering. *Physica B* **2004**, *350*, E763-E766.
67. Kampmann, R.; Haese-Seiller, M.; Kudryashov, V.; Nickel, B.; Daniel, C.; Fenzl, W.; Schreyer, A.; Sackmann, E.; Rädler, J. Horizontal ToF-Neutron Reflectometer REFSANS at FRM-II Munich/Germany: First Tests and Status. *Physica B* **2006**, *385-386*, 1161–1163.
68. Nelson, A. Co-Refinement of Multiple-Contrast Neutron/X-ray Reflectivity Data Using MOTOFIT. *J. Appl. Crystallogr.* **2006,** *39*, 273−276.
69. Sears, V. F. Neutron Scattering Lengths and Cross Sections. *Neutron News* **2006**, *3*, 26–37.
70. Wang, W.; Kaune, G.; Perlich, J.; Papadakis, C. M.; Bivigou Koumba, A. M.; Laschewsky, A.; Schlage, K.; Röhlsberger, R.; Roth, S. V.; Cubitt, R.; Müller-Buschbaum, P. Swelling and Switching Kinetics of Gold Coated End-capped Poly(N -isopropylacrylamide) thin films. *Macromolecules* **2010**, *43*, 2444–2452.
71. Wang, W.; Troll, K.; Kaune, G.; Metwalli, E.; Ruderer, M.; Skrabania, K.; Laschewsky, A.; Roth, S. V.; Papadakis, C. M.; Müller-Buschbaum, P. Thin Films of Poly(N-isopropylacrylamide) End-Capped with n-Butyltrithiocarbonate. *Macromolecules* **2008**, *41*, 3209–3218.
72. Harms, S.; Rätzke, K.; Faupel, F.; Egger, W.; Ravello, L.; Laschewsky, A.; Wang, W.; Müller-Buschbaum, P. Free Volume and Swelling in Thin Films of Poly(N-isopropylacrylamide) End-Capped with n-Butyltrithiocarbonate. *Macromol. Rapid Commun.* **2010**, *31*, 1364–1367.
73. Sun, Q. The Raman OH Stretching Bands of Liquid Water. *Vib. Spectrosc.* **2009**, *51*, 213–217.
74. Vyumvuhore, R.; Tfayli, A.; Duplan, H.; Delalleau, A.; Manfait, M.; Baillet-Guffroy, A. Effects of Atmospheric Relative Humidity on Stratum Corneum Structure at the Molecular Level: Ex Vivo Raman Spectroscopy analysis. *Analyst* **2013**, *138*, 4103–4111

Supporting Information

Cyclic Water Storage Behavior of Doubly Thermo-responsive Poly(sulfobetaine)-Based Diblock Copolymer Thin Films

Lucas P. Kreuzer[†], Tobias Widmann[†], Nawarah Aldosari[†], Lorenz Bießmann[†], Gaetano Mangiapia[§], Viet Hildebrand[‡], André Laschewsky[‡,⊥], Christine M. Papadakis[†], Peter Müller-Buschbaum[†,$,]*

[†]Lehrstuhl für Funktionelle Materialien, Physik Department, Technische Universität München, James-Franck-Str. 1, 85748 Garching, Germany

[§]Helmholtz-Zentrum Geesthacht at Heinz Maier-Leibnitz Zentrum, Lichtenbergstr. 1, 85747 Garching, Germany

[‡]Institut für Chemie, Universität Potsdam, Karl-Liebknecht-Str. 24-25, 14476 Potsdam-Golm, Germany

[⊥]Fraunhofer Institut für Angewandte Polymerforschung, Geiselbergstr. 69, 14476 Potsdam-Golm, Germany

[$]Heinz Maier-Leibnitz Zentrum (MLZ), Technische Universität München, Lichtenbergstr. 1, 85748 Garching, Germany

* E-mail corresponding author: muellerb@ph.tum.de

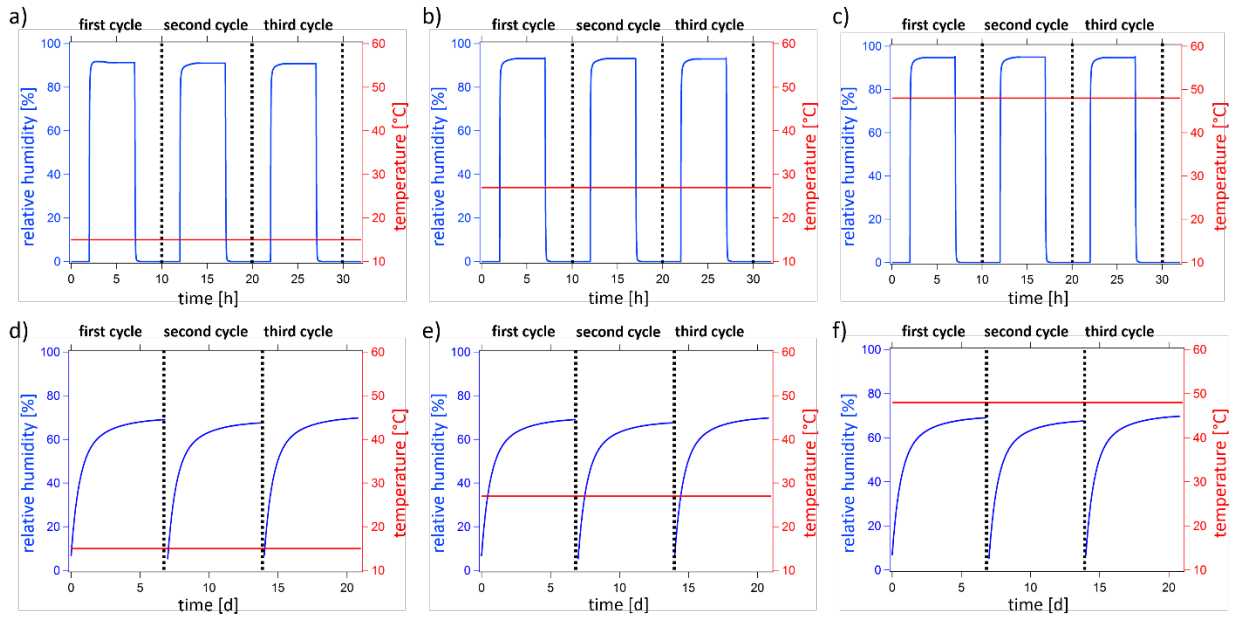

Figure S1: Relative humidity (blue) and temperature (red) as function of time for the three swelling and collapse cycles during the (a-c) ToF-NR and (d-f) FTIR measurements at (a, d) 15 °C, (b, e) 27 °C, and (c, f) 48 °C. One full cycle is defined as static measurement at 0 % relative humidity, a kinetic measurement following the swelling process, a static measurement at high humidity, a kinetic measurement following the drying process, and a final static measurement at 0 % relative humidity.

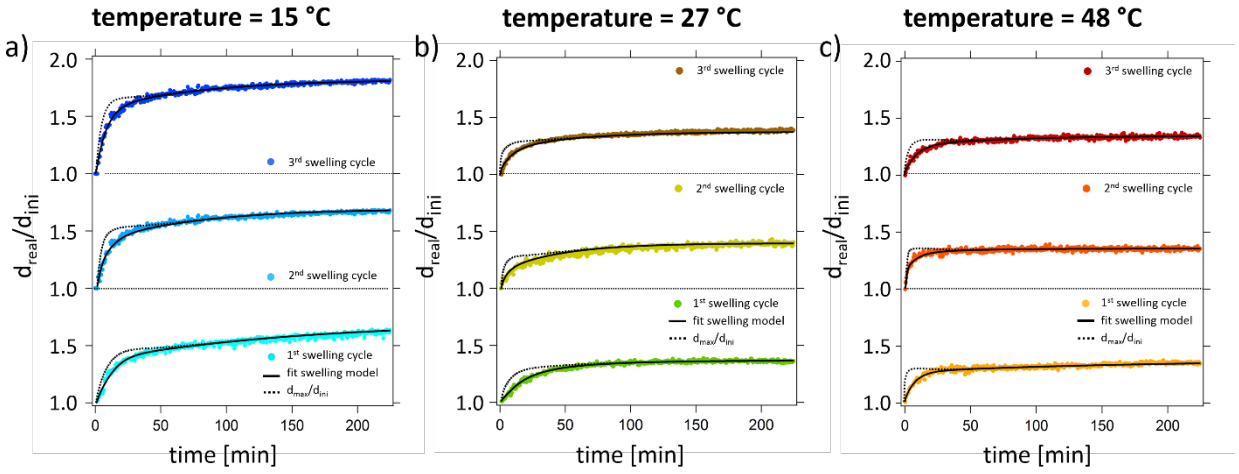

Figure S2: Swelling ratio d_{real}/d_{ini} as a function of time followed with SR over three swelling cycles at 15 °C (a), 27 °C (b), and 48 °C (c), respectively. The cycle number increases from bottom (first cycle) to top (third cycle). The temporal evolution of the swelling ratio d_{real}/d_{ini} is fitted with a swelling model as explained in the main text (black line). Furthermore, the maximum swelling ratio $d_{\max}/d_{ini}$ is plotted (dashed black line).

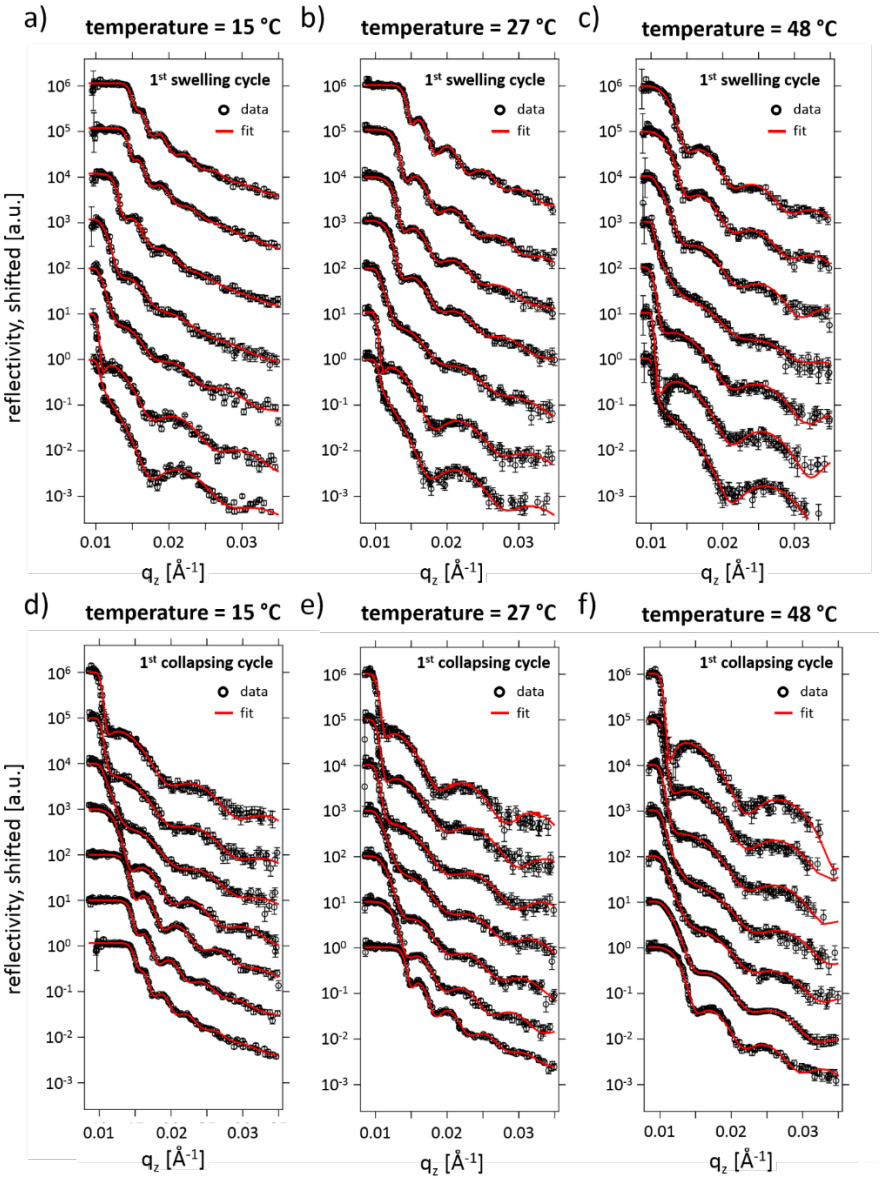

Figure S3: Selected NR data (black circles) and the corresponding fits (red lines) for the first swelling cycle at 15 °C (a), 27 °C (b), and 48 °C (c) as well as for the first collapsing cycle at 15 °C (d), 27 °C (e), and 48 °C (f). For the first swelling cycles (a-c) the NR curves are taken at t = 0, 2, 5, 8, 10, 15, and 100 min. The NR curves for the first collapsing cycles at 15 °C and 48 °C (d and f) are taken at t = 0, 10, 20, 30, 45, 60 and 100 minutes, whereas for the first collapsing cycle at 27 °C the selected reflectivity curves are taken at t = 0, 1.5, 3, 5, 8, 10 and 100 min.

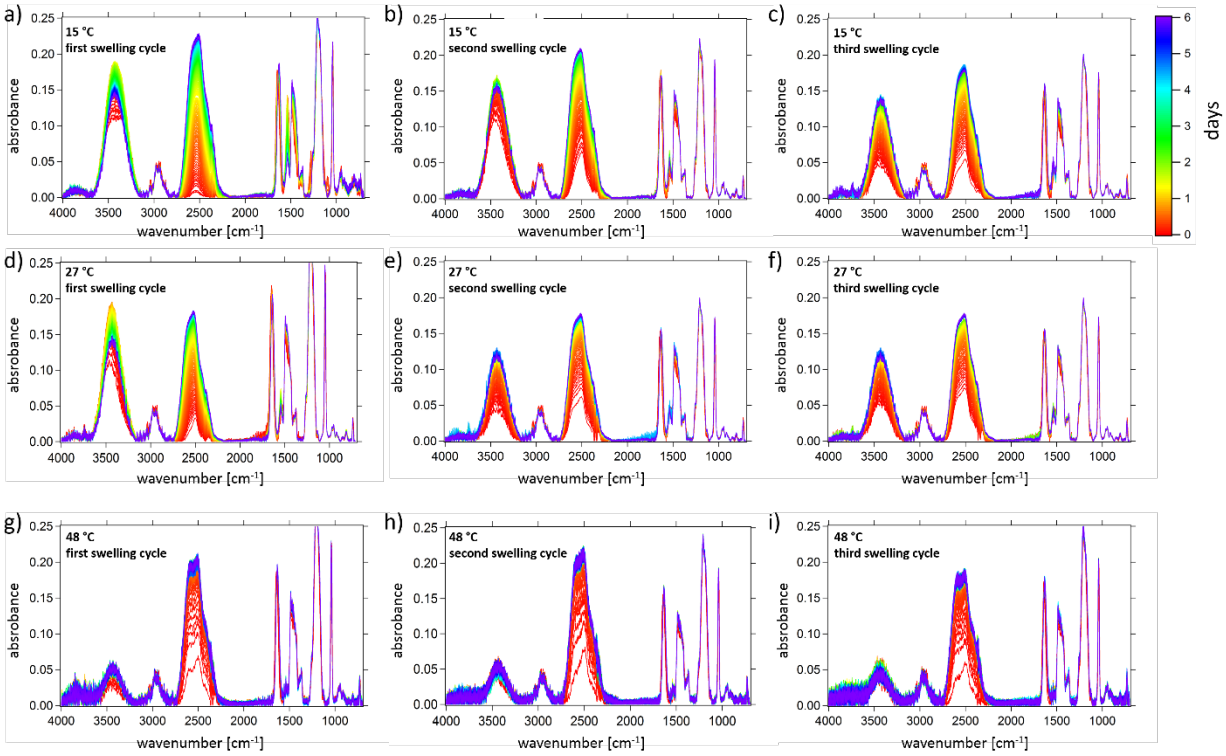

Figure S4: FTIR spectra of in total three swelling cycles at 15 °C (a-c), 27 °C (d-f), and 48 °C (g- i), respectively. The number of cycles increases from left to right. The time is encoded in the color of the FTIR spectra as indicated.

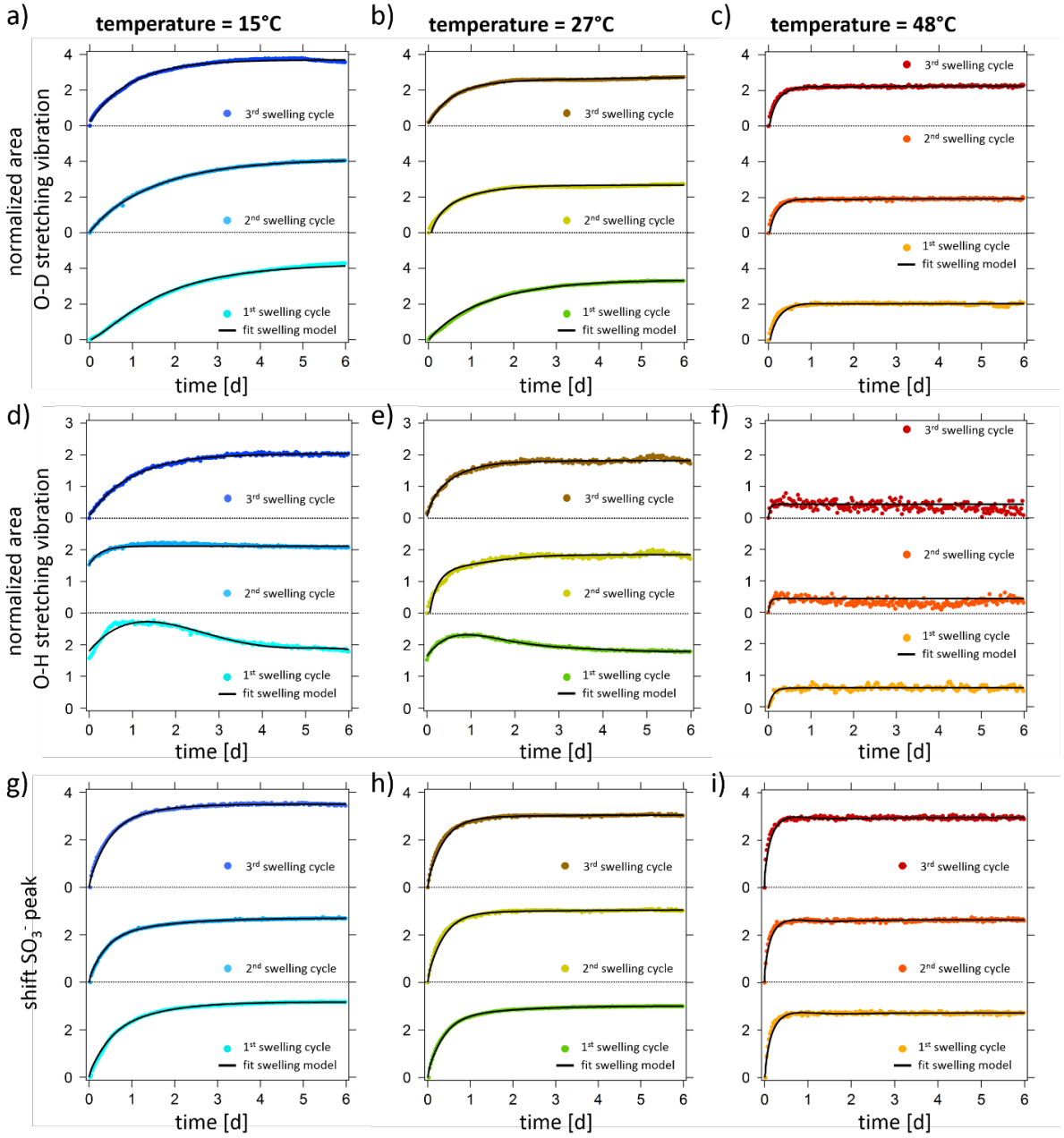

Figure S5: Normalized area of the O-D stretching vibration at 15 °C (a), 27 °C (b), and 48 °C (c), normalized area of the O-H stretching vibration at 15 °C (d), 27 °C (e), and 48 °C (f), and shift of the SO_3^- peak maximum at 15 °C (g), 27 °C (h), and 48 °C (i) as extracted from the FTIR spectra. The cycle number increases from bottom (first cycle) to top (third cycle). The curves are fitted with the swelling model as explained in the main text (black line).

Table S1: Values of χ_{eff} and τ for the respective swelling cycles at 15 °C. 27 °C, and 48 °C, obtained with SR as is shown in Figure S2.

	swelling	
15 °C	χ_{eff}	τ / min
first cycle	0.60 ± 0.02	30 ± 1
second cycle	0.62 ± 0.02	28 ± 2
third cycle	0.61 ± 0.03	31 ± 1
27 °C		
first cycle	0.91 ± 0.02	20 ± 1
second cycle	0.92 ± 0.01	20 ± 1
third cycle	0.92 ± 0.03	22 ± 2
48 °C		
first cycle	1.12 ± 0.04	16 ± 1
second cycle	1.08 ± 0.04	17 ± 1
third cycle	1.09 ± 0.03	17 ± 1

Table S2: Values of χ_{eff} and τ for the respective swelling cycles at 15 °C. 27 °C, and 48 °C, obtained with ToF-NR as is shown in Figure 3 in the main text.

	determined from d/d_{ini} *vs* t		determined from Φ *vs* t	
15 °C	χ_{eff}	τ / min	χ_{eff}	τ / min
first cycle	0.32 ± 0.02	11 ± 1	0.14 ± 0.01	12 ± 1
second cycle	0.32 ± 0.01	10 ± 1	0.15 ± 0.01	13 ± 1
third cycle	0.33 ± 0.01	10 ± 1	0.14 ± 0.02	13 ± 1
27 °C				
first cycle	0.52 ± 0.01	7 ± 1	0.42 ± 0.02	6 ± 1
second cycle	0.54 ± 0.01	6 ± 1	0.41 ± 0.03	5 ± 1
third cycle	0.52 ± 0.01	6 ± 1	0.41 ± 0.02	6 ± 1
48 °C				
first cycle	0.65 ± 0.03	6 ± 1	0.55 ± 0.02	5 ± 1
second cycle	0.66 ± 0.02	6 ± 1	0.55 ±0.03	4 ± 1
third cycle	0.66 ± 0.02	6 ± 1	0.54 ± 0.02	4 ± 1

Table S3: Values of χ_{eff} and τ for the respective drying cycles at 15 °C. 27 °C, and 48 °C, obtained with ToF-NR as is shown in Figure 5 in the main text.

	determined from d/d_{ini} vs time		determined from Φ vs time	
15 °C	χ_{eff}	τ / min	χ_{eff}	τ / min
first cycle	0.91 ± 0.03	21 ± 2	1.08 ± 0.04	35 ± 4
second cycle	0.92 ± 0.04	22 ± 3	1.09 ± 0.04	36 ± 4
third cycle	0.89 ± 0.04	21 ± 3	1.09 ± 0.03	36 ± 3
27 °C				
first cycle	1.11 ± 0.04	6 ± 1	1.31 ± 0.04	10 ± 1
second cycle	1.08 ± 0.03	8 ± 2	1.29 ± 0.04	9 ± 1
third cycle	1.08 ± 0.03	8 ± 1	1.29 ± 0.03	10 ± 1
48 °C				
first cycle	1.21 ± 0.05	15 ± 1	1.42 ± 0.04	24 ± 1
second cycle	1.18 ± 0.05	14 ± 2	1.42 ± 0.05	24 ± 1
third cycle	1.20 ± 0.06	14 ± 2	1.39 ± 0.04	23 ± 2

Table S4: Values of χ_{eff} and τ for the respective swelling cycles at 15 °C. 27 °C, and 48 °C, obtained with FTIR as is shown in Figure 7.

	Determined from O-D stretching vibration vs time		Determined from O-H stretching vibration vs time		Determined from SO_3^- maximum peak position vs time	
	χ_{eff}	τ / d	χ_{eff}	τ / d	χ_{eff}	τ / d
15 °C						
first cycle	0.51 ± 0.03	3.1 ± 0.2	0.45 ± 0.02	2.4 ± 0.2	0.31 ± 0.03	91 ± 4
second cycle	0.51 ± 0.02	2.7 ± 0.1	0.44 ± 0.02	1.6± 0.02	0.31 ± 0.02	92 ± 5
third cycle	0.53 ± 0.02	2.8 ± 0.1	0.44 ± 0.02	1.6 ± 0.02	0.33 ± 0.02	90 ± 5
27 °C						
first cycle	1.02 ± 0.04	1.8 ± 0.1	0.95 ± 0.03	1.8 ± 0.2	0.73 ± 0.05	57 ± 3
second cycle	1.01 ± 0.04	1.3 ± 0.1	0.94 ± 0.02	1.1 ± 0.02	0.73 ± 0.04	57 ± 3
third cycle	1.00 ± 0.05	1.3 ± 0.1	0.95 ± 0.02	1.1 ± 0.02	0.75 ± 0.04	55 ± 4
48 °C						
first cycle	1.22 ± 0.06	0.5 ± 0.1	1.13 ± 0.04	0.1 ± 0.03	0.98 ± 0.05	26 ± 3
second cycle	1.22 ± 0.07	0.5 ± 0.1	1.12 ± 0.03	0.1 ± 0.03	1.01 ± 0.05	24 ± 3
third cycle	1.24 ± 0.05	0.5 ± 0.1	1.12 ± 0.03	0.1 ± 0.03	0.99 ± 0.06	24 ± 2

Model for swelling process in thin films

Detailed information about the swelling model, which is based on the work of Li and Tanaka[1] as well as on the work of Jaczewska et al.[2], and the application to the data can be found in our previous publications.[3-5] The main text refers to the following equations:

Equation S1 describes the diffusion of water molecules into the DBC thin film often described as intrinsic swelling kinetic

$$\frac{d(t)}{d_{ini}} = \frac{d_{\max}}{d_{ini}} - \left(\frac{d_{\max}}{d_{ini}} - 1\right) B \exp\left(-\frac{t}{\tau}\right) \tag{S1}$$

d_{ini} is the initial film thickness of the $PSPP_{500}$-b-$PNIPMAM_{150}$ thin film in its as-prepared state at a measurement time t. τ represents the timescale on which the kinetic process is happening. B is related to the sample geometry (it is between 0.75 and 1 for thin films). $d_{\max}/d_{ini}$ stands for the maximum swelling ratio and is determined by Equation S2

$$\frac{d_{\max}}{d_{ini}} = \frac{\frac{d(t)}{d_{ini}} - B\exp\left(-\frac{t}{\tau}\right)}{1 - B\exp\left(-\frac{t}{\tau}\right)} \tag{S2}$$

The non-constant relative humidity is considered as

$$\ln\left(\frac{p}{p_{sat}}\right) = \ln\left(1 - \frac{d_{ini}}{d_{\max}}\right) + \left(1 - \frac{V_{water}}{V_{polymer}}\right)\frac{d_{ini}}{d_{\max}} + \chi_{eff}\left(\frac{d_{ini}}{d_{\max}}\right)^2 \tag{S3}$$

p/p_{sat} represents a changing relative humidity, V_{water} and $V_{polymer}$ are the molar volumes of water and the polymer. χ_{eff} is the effective Flory-Huggins parameter between two components and is a measure for the hydrophilicity of the DBC. Eq. S1 and Eq. S3 are combined by solving Eq. S1 for the maximum swelling ratio and insert it in Eq. S3. The resulting implicit function is solved numerically for the swelling ratio, dependent on the measurement time. In a last step, $d(t)$ is

substituted with $\Phi(t)$ according to Equation S4 in order to be able to also fit the water content $\Phi(t)$:

$$\frac{d(t)}{d_{ini}} = \frac{1}{1-\Phi(t)} \tag{S4}$$

References

(1) Li, Y.; Tanaka, T. Kinetics of Swelling and Shrinking of Gels. *The Journal of Chemical Physics* **1990**, *92*, 1365–1371.

(2) Jaczewska, J.; Raptis, I.; Budkowski, A.; Goustouridis, D.; Raczkowska, J.; Sanopoulou, M.; Pamuła, E.; Bernasik, A.; Rysz, J. Swelling of Poly(3-alkylthiophene) Films Exposed to Solvent Vapors and Humidity. *Synthetic Metals* **2007**, *157*, 726–732.

(3) Kreuzer, L. P.; Widmann, T.; Hohn, N.; Wang, K.; Bießmann, L.; Peis, L.; Moulin, J.-F.; Hildebrand, V.; Laschewsky, A.; Papadakis, C. M.; Müller-Buschbaum, P. Swelling and Exchange Behavior of Poly(sulfobetaine)-Based Block Copolymer Thin Films. *Macromolecules* **2019**, *52*, 3486–3498.

(4) Widmann, T.; Kreuzer, L. P.; Hohn, N.; Bießmann, L.; Wang, K.; Rinner, S.; Moulin, J.-F.; Schmid, A. J.; Hannappel, Y.; Wrede, O.; Kühnhammer, M.; Hellweg, T.; Klitzing, R. von; Müller-Buschbaum, P. Hydration and Solvent Exchange Induced Swelling and De-Swelling of Homogeneous Poly(N-isopropylacrylamide) Microgel Thin Films. *Langmuir* **2019**.

(5) Kreuzer, L. P.; Widmann, T.; Bießmann, L.; Hohn, N.; Pantle, J.; Märkl, R.; Moulin, J.-F.; Hildebrand, V.; Laschewsky, A.; Papadakis, C. M.; Müller-Buschbaum, P. Phase Transition Kinetics of Doubly Thermoresponsive Poly(sulfobetaine)-Based Diblock Copolymer Thin Films. *Macromolecules* **2020**, *53*, 2841–2855.